

1 **Dissolved and suspended organic matter dynamics in the Cape Verde Frontal Zone**
2 **(NW Africa)**

3 S. Valiente^{a,b}, B. Fernández-Castro^{b,c}, R. Campanero^{a,b}, A. Marrero-Díaz^d, A.
4 Rodríguez-Santana^d, M.D. Gelado-Cabellero^e, M. Nieto-Cid^{b,f}, A. Delgado-Huertas^a, J.
5 Arístegui^g, X.A. Álvarez-Salgado^b

6
7 ^a CSIC Instituto Andaluz de Ciencias de la Tierra (IACT–CSIC), Granada, Spain

8 ^b CSIC Instituto de Investigaciones Mariñas (IIM–CSIC), Vigo, Spain

9 ^c Ocean and Earth Science, National Oceanography Center Southampton, University of Southampton,
10 Southampton, UK

11 ^d Departamento de Física, Universidad de Las Palmas de Gran Canaria, Las Palmas de Gran Canaria,
12 Spain

13 ^e Departamento de Química, Universidad de Las Palmas de Gran Canarias, Las Palmas, Spain

14 ^f Instituto Español de Oceanografía (IEO), Centro Oceanográfico de A Coruña, A Coruña, Spain

15 ^g Instituto de Oceanografía y Cambio Global, Universidad de Las Palmas de Gran Canaria, Telde, Spain

16
17 **Abstract**

18 The Cape Verde Frontal Zone (CVFZ) is a highly dynamic region located in the
19 southern boundary of the Canary Current Eastern Boundary Upwelling Ecosystem. Due
20 to the interaction of the Cape Verde Front with the Mauritanian coastal upwelling, the
21 area features large vertical and horizontal export fluxes of organic matter. While the
22 flux, composition and biogeochemical role of sinking organic matter have been
23 thoroughly studied, much less attention has been paid to the dissolved (DOM) and
24 suspended particulate (POM) organic matter fractions. Full-depth profiles of DOM and
25 POM were recorded during an oceanographic cruise in the CVFZ, with four consecutive
26 transects defining a box embracing the giant filament of Cape Blanc and the Cape Verde
27 front. The distributions of DOM and POM and their C:N stoichiometric ratios in the
28 epipelagic layer were strongly influenced by the position of the transects relative to the
29 giant filament and the front. Geographical heterogeneity in POM and DOM
30 distributions and elemental composition was also observed within each of the different
31 water masses of contrasting origin present in the area (North and South Atlantic Central
32 Water, Subpolar Mode Water, Mediterranean Water, Antarctic Intermediate Water,
33 Labrador Sea Water and North East Atlantic Deep Water). **These facts suggest that**
34 **water masses properties are re-shaped by biogeochemical processes occurring within the**
35 **CVFZ. Nevertheless, our analysis indicates that DOM and POM mineralisation**

36 represents only 8.1% of the inorganic carbon and 17.8% of the inorganic nitrogen
37 produced by the local mineralisation of organic matter. Intense lateral export of POM
38 and DOM out of the boundaries of the CVFZ is the likely reason behind these low
39 contributions, which confirm the prominent role of sinking fluxes of organic matter for
40 mineralisation processes in this region. The DOM distribution in the CVFZ interior is
41 apparently affected by the dissolution of fast sinking particles.

42
43 **Keywords:** Dissolved organic matter; particulate organic matter; water masses; carbon
44 cycling; nitrogen cycling; Cape Verde Frontal Zone

45 46 **List of acronyms**

AA	Modified Antarctic Intermediate Water
AOU	Apparent oxygen utilization
Chl-a	Chlorophyll a
CVF	Cape Verde Front (when referring exclusively to the Front)
CVFZ	Cape Verde Frontal Zone (when referring to the entire study area)
DCM	Deep chlorophyll maximum
DOC	Dissolved organic carbon
DOM	Dissolved organic matter
DON	Dissolved organic nitrogen
EBUE	Eastern Boundary Upwelling Ecosystem
ENACW	Eastern North Atlantic Central Water
ENACW_15	Eastern North Atlantic Central Water of 15 °C
ENACW_12	Eastern North Atlantic Central Water of 12 °C
LNEADW	Lower North East Atlantic Deep Water
LSW	Labrador Sea Water
MMW	Madeira Mode Water
MW	Mediterranean Water
NEADW	North East Atlantic Deep Water
NO	Conservative chemical parameter, obtained as $NO = O_2 + R_N \cdot NO_3^-$
OMP	Optimum multiparameter analysis
POC	Particulate organic carbon
POM	Particulate organic matter
PON	Particulate organic nitrogen
R _N	Stoichiometric conversion factor of nitrate to dissolved oxygen, 9.3 mol O ₂ mol NO ₃ ⁻¹
SACW	South Atlantic Central Water
SACW_12	South Atlantic Central Water of 12°C
SACW_18	South Atlantic Central Water of 18°C
SE	Standard error
SPMW	Subpolar Mode Water
TDN	Total dissolved nitrogen
UNEADW	Upper North East Atlantic Deep Water

47 **1. Introduction**

48 The Eastern Boundary Upwelling Ecosystem (EBUE) associated with the Canary
49 Current extends from the northern tip of the Iberian Peninsula at 43°N to South of
50 Senegal at about 10°N (Aristegui et al., 2009). The intensity and persistence of
51 upwelling-favourable winds increase with decreasing latitude, evolving from weak and
52 seasonal to the North to strong and year-round to the South. The Canary Current EBUE
53 is also characterized by an intense mesoscale activity in the form of upwelling filaments
54 associated with prominent capes (Álvarez-Salgado et al., 2007; Lovecchio et al., 2018;
55 Santana-Falcón et al., 2020) and island eddies (Barton et al., 1998; Sangrà et al., 2009;
56 Cardoso et al., 2020). These mesoscale structures may export large amounts of organic
57 matter produced over the shelf several hundreds of kilometres offshore (Gabric et al.,
58 1993; Ohde et al., 2015; Lovecchio et al., 2018). Mesoscale activity is particularly
59 intense in the southern boundary of the Canary Current EBUE due to the confluence of
60 the Mauritanian upwelling and the Cape Verde Front (CVF). The CVF separates the
61 eastern margins of the subtropical and tropical Atlantic gyres (Pelegrí and Peña-
62 Izquierdo, 2015) and favours the horizontal transport from the coast, contributing to
63 developing the giant filament of Cape Blanc (21°N). This structure exports offshore
64 massive amounts of biogenic organic matter produced in the Mauritanian coast (Van
65 Camp et al., 1991; Gabric et al., 1993). At the CVF, Eastern North Atlantic Central
66 Water (ENACW) encounters the slightly cooler, less saline, nutrient-richer and oxygen-
67 poorer South Atlantic Central Water (SACW) (Zenk et al., 1991). In the frontal region,
68 intense interleaving between the two water masses occurs (Pérez-Rodríguez et al., 2001;
69 Martínez-Marrero et al., 2008), as well as the recurrent formation of meanders and
70 eddies (Meunier et al., 2012; Alpers et al., 2013).

71
72 Upwelling filaments, meandering fronts and eddies affect the distribution and net
73 community production of surface plankton communities in the Cape Verde Frontal
74 Zone (CVFZ) (Olivar et al., 2016; Tiedemann et al., 2018; Aristegui et al., 2020). The
75 organic matter transported by these structures is dominated by small suspended or slow
76 sinking particulate organic matter, hereinafter suspended POM, and dissolved organic
77 matter (DOM), while fast sinking POM (generally >100 µm) is less susceptible to
78 horizontal advection (Álvarez-Salgado and Aristegui, 2015). Differentiation between
79 suspended and sinking POM is of fundamental importance because of the contrasting
80 mechanisms involved in their dispersion (horizontal export for suspended POM vs.

1
2
3
4
5
6
7
8
9
10
11
12
13
14
15
16
17
18
19
20
21
22
23
24
25
26
27
28
29
30
31
32
33
34
35
36
37
38
39
40
41
42
43
44
45
46
47
48
49
50
51
52
53
54
55
56
57
58
59
60
61
62
63
64
65

81 vertical export for sinking POM) and fate during offshore transport from the coast to the
82 ocean interior (Helmke et al., 2005; Fischer et al., 2009; Álvarez-Salgado and Arístegui,
83 2015). While suspended POM, is generally collected with Niskin bottles or stand-alone
84 pumps, fast sinking POM is collected with sediment traps. POM is differentiated from
85 DOM as the fraction of marine organic matter retained by a filter of a given pore size
86 that usually range from 0.2 μm (polycarbonate, polysulfone, or aluminium filters) to 0.7
87 μm (typically glass fibber filters; Repeta, 2015). The CVFZ is characterized by the
88 lateral export of organic matter from the coast to the open ocean not only in the surface
89 nepheloid layer (SNL) but also in intermediate (INL) and bottom (BNL) nepheloid
90 layers (Karakaş et al., 2006; Nowald et al., 2006; Fischer et al., 2009; Ohde et al.,
91 2015), which affects carbon fluxes in the adjacent deep ocean waters (Alonso-González
92 et al., 2009; Arístegui et al., 2020).

93
94 Information on the elemental composition of DOM, and suspended and sinking
95 POM is crucial to understand the contrasting contribution of the three organic matter
96 pools to the respiration in the ocean interior, which dictates the efficiency and
97 magnitude of the biological carbon pump (Verdugo et al., 2004; Hopkinson and Vallino,
98 2005; Boyd et al., 2019). While an important effort has been made to characterize the
99 origin, elemental composition and fluxes of sinking POM in the CVFZ (Helmke et al.,
100 2005; Iversen et al., 2010; Álvarez-Salgado and Arístegui, 2015 and references therein;
101 Fischer et al., 2019), the suspended POM and DOM fractions received much less
102 attention (Alonso-González et al., 2009; Arístegui et al., 2020; Burgoa et al., 2020).
103 Therefore the aim of this work is to study the dynamics of the dissolved and suspended
104 fractions of organic matter in the CVFZ, and quantify the contribution of these pools to
105 the remineralisation of organic matter in the dark ocean. Full-depth profiles of the
106 carbon (C) and nitrogen (N) content of DOM and suspended POM were obtained in a
107 box (17-23°N, 17-26°W) that embraced the giant filament of Cape Blanc and the CVF.
108 Differences in dissolved organic carbon (DOC) and suspended particulate organic
109 carbon (POC) stocks, C:N molar ratios, and their relative contribution to dissolved
110 oxygen consumption and nitrate production following organic matter mineralisation
111 between transects (Northern, NACW domain; Southern, SACW domain; Eastern,
112 Coastal Transition Zone domain; and Western, open ocean domain) are examined for
113 the surface, central, intermediate and deep water masses present in the study area.

115 2. Materials and Methods

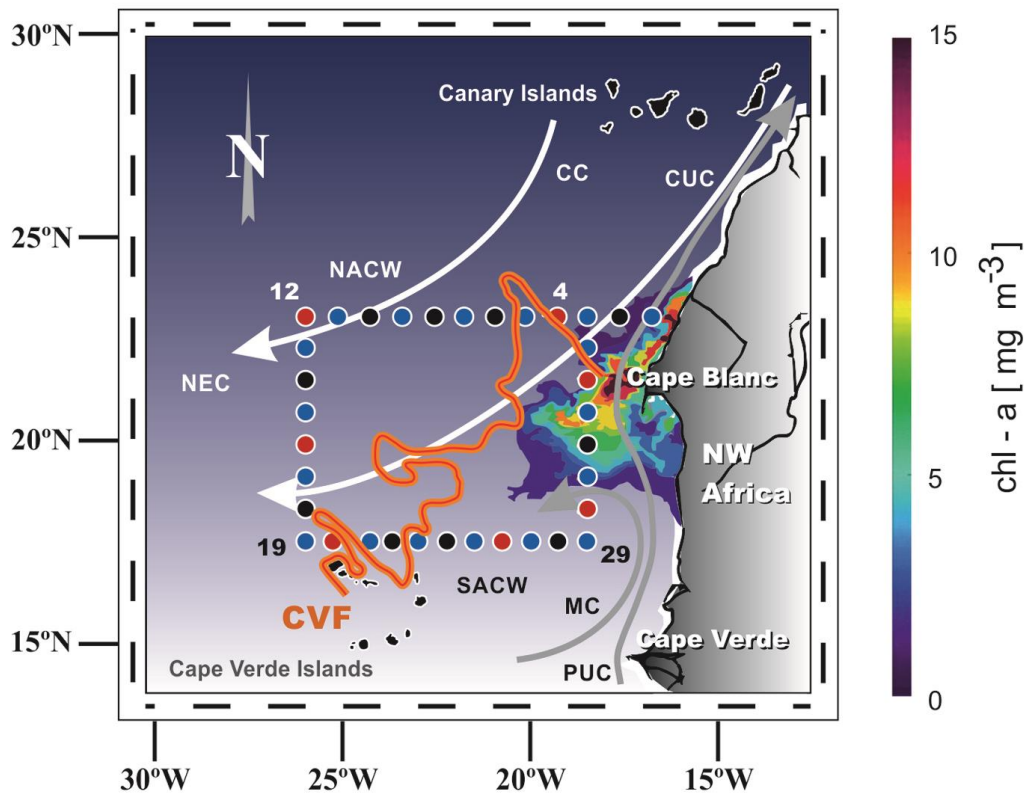
116 2.1. Sampling strategy

117 The FLUXES I cruise (R/V Sarmiento de Gamboa; Las Palmas - Las Palmas, 12
118 July to 9 August 2017) consisted of four transects (Northern, Western, Southern and
119 Eastern) defining a box crossing the CVFZ, including 35 hydrographic stations 50
120 nautical miles apart (Figure 1). Three types of stations were occupied: short (nocturnal),
121 medium (diurnal) and long (full day), which lasted 3, 9 and 27 hours, respectively
122 (Figure 1). Medium and long stations were sampled from the surface to 4000 db,
123 whereas short stations were sampled down to 2000 db. A rosette sampler carrying 24
124 Niskin bottles of 12 litres was used. It was equipped with a conductivity, temperature
125 and depth (CTD) probe (SeaBird SBE911 plus), and sensors for dissolved oxygen
126 (SeaBird SBE43), fluorescence of chlorophyll (SeaPoint SCF), and turbidity (SeaPoint
127 STM). Sampling depths were selected based on the continuous records of the sensors
128 attached to the rosette. Fifteen levels were sampled in medium and long stations (down
129 to 4000 db) and 10 levels in short stations (down to 2000 db).

130
131 CTD conductivity was calibrated with water samples taken from the rosette and
132 analysed on board with a Guildline 8410-A Portasal salinometer. Samples for dissolved
133 oxygen (O₂) determination were analysed on board by the Winkler potentiometric
134 method following the procedure described by Langdon (2010). The apparent oxygen
135 utilization (AOU) was calculated with the equation of Benson & Krause, $AOU = O_{2sat} -$
136 O_2 (UNESCO, 1986), where O_{2sat} is the dissolved oxygen saturation at local TS. The
137 chlorophyll (Chl) fluorescence sensor was calibrated with water samples taken at 4
138 depths in the photic layer at each medium and long stations, where 500 mL of water was
139 filtered and phytoplankton cells concentrated on 25 mm GF/F filters for chlorophyll a
140 determination. Pigments were extracted with 10 mL of 90% acetone at 4°C in the dark
141 for 24 h. The extracts were estimated fluorometrically by means of a Turner Designs
142 bench fluorometer 10-AU, previously calibrated with pure chlorophyll a (Sigma Co.), as
143 described in Holm-Hansen et al. (1965).

144
145 Water samples for the determination of inorganic nutrient concentrations were
146 taken directly from the Niskin bottles in 25 mL polyethylene vials that were frozen at -
147 20°C until analysis in the base laboratory. A similar procedure was followed for
148 dissolved organic carbon / total dissolved nitrogen (DOC / TDN) samples, which were

149 collected in 30 mL amber glass vials with Teflon stoppers. Although these samples
 150 were not filtered, they will be named as DOC and TDN, because they mainly represent
 151 DOM due to the low concentrations of POM in oceanic waters. For the analysis of the
 152 concentration of **suspended** particulate organic carbon and nitrogen (POC and PON), 2
 153 to 5 L of water were filtered onto pre-combusted (450°C, 4 hours) 25 mm Whatman
 154 GF/F filters in a filtration system with a mild vacuum (pressure difference <300 mm
 155 Hg). Filters were transferred to 2 mL Eppendoff vials and dried for 12 hours in a
 156 vacuum desiccator with silica gel. After drying, they were frozen at -20°C until analysis
 157 in the base laboratory. Dissolved oxygen, inorganic nutrients, DOC/TDN and
 158 POC/PON were collected at all stations and all sampling depths.



159 Figure 1. Map of the FLUXES I cruise. The dots represent the stations (blue: diurnal stations; black:
 160 nocturnal stations; red: long stations) the numbers indicate the station number, from 1 to 35. The main
 161 geographic and oceanographic features and currents are represented. The white arrows correspond to the
 162 Canary Current (CC), Canary Upwelling Current (CUC) and North Equatorial Current (NEC), the grey
 163 arrows to the Mauritania Current (MC) and the Poleward Undercurrent (PUC) (taken from Pelegrí and
 164 Peña-Izquierdo, 2015). The orange line represents the approximate position of the CVF during the cruise
 165 (taken from Burgoa et al. in review), and the colour contours near the coast represent the satellite
 166 chlorophyll *a* associated with the Cape Blanc filament on 24/07/2017 (from Copernicus Marine Service).
 167
 168

169 2.2. Analytical determinations

170 Micromolar concentrations of nutrient salts (nitrate, nitrite, ammonium, phosphate
 171 and silicate) were determined simultaneously by segmented flow analysis in an Alliance

172 Futura autoanalyser following the methods of Hansen and Koroleff (1999) except for
173 the case of ammonium, which was measured by the fluorometric method of K  rouel and
174 Aminot (1997). Frozen samples were gently melted in the dark overnight and
175 vigorously shaken before analytical determination.

177 The determination of **suspended** POC and PON in 25 mm GF/F filters was carried
178 out by high temperature catalytic oxidation at 900  C in a Perkin Elmer 2400 elemental
179 analyser. At two selected stations, one from the Eastern (coastal) and one from the
180 Western (open ocean) transects, the filters were divided into two parts; one part was
181 measured directly and the other part was exposed to HCl fumes for 24 hours to remove
182 CaCO₃ before determination. After checking that CaCO₃ represented <10% of carbon in
183 these filters, the rest of the filters were analysed directly. Therefore, although we have
184 measured total carbon, we will refer to these measurements as POC because of the low
185 levels of CaCO₃.

187 DOC and TDN were analysed by high temperature catalytic oxidation at 680  C
188 with a Shimadzu TOC-V analyser connected in line with a TNM1 measuring unit. After
189 melting, the samples were acidified to pH <2 and degassed with high purity N₂ to
190 eliminate the CO₂ before measurement. Aliquots of 150   L were injected in the
191 analyser. Measurements were made in triplicate to quintuplicate. The accuracy was
192 checked daily with the DOC/TDN reference materials (CRM) provided by D.A. Hansell
193 (University of Miami, USA). Measured concentrations of the CRM were 44.9    1.7
194   mol C L⁻¹ (n = 10) and 31.7    1.4   mol N L⁻¹ (n = 10); the certified values are 43–45
195   mol C L⁻¹ and 32–33   mol N L⁻¹ (DSW Batch 16–2016*Lot 05-16). DON
196 concentrations were calculated as DON = TDN - DIN where DIN is the dissolved
197 inorganic nitrogen (nitrate + nitrite + ammonium).

199 **2.3. Water mass analysis**

200 An optimum multiparameter (OMP) inverse method (Karstensen and Tomczak,
201 1998) has been used for the quantification of the water types (WTs) that contribute to
202 the water samples collected in the CVFZ during FLUXES I. A water type (WT) is a
203 body of water formed in a particular region of the ocean with certain thermohaline and
204 chemical properties (Tomczak, 1999).

206 In our OMP, the variables used to define the WTs were potential temperature (θ),
 207 salinity (S), silicate (SiO_4H_4) and the conservative chemical parameter NO ($\text{NO} = \text{O}_2 +$
 208 $R_N \cdot \text{NO}_3^-$ (Broecker, 1974) where R_N was set to a constant value of $9.3 \text{ mol O}_2 \text{ mol NO}_3^-$
 209 $^{-1}$ (Anderson, 1995)), and represents the Redfield ratio of dissolved oxygen consumption
 210 to nitrate production during the mineralisation of biogenic organic matter in the ocean.
 211 We identified 11 WT in the CVFZ: Madeira Mode Water (MMW); Eastern North
 212 Atlantic Central Water (ENACW) of 15°C and 12°C ; South Atlantic Central Water of
 213 18°C and 12°C ; Subpolar Mode Water (SPMW); Antarctic Intermediate Water (AA);
 214 Mediterranean Water (MW); Labrador Sea Water (LSW); and upper and lower North
 215 East Atlantic Deep Water (NEADW). The physical and chemical properties of most of
 216 these WTs were obtained from the literature (Table 1), except for AA and SACW of
 217 18°C and 12°C , which were defined from the average characteristics of these WTs in the
 218 Eastern Equatorial Atlantic, between 5°N – 5°S and 20 – 30°W (World Ocean Atlas,
 219 2013). This source region was chosen because AA and SACW are transported from the
 220 Equatorial Atlantic to the CVFZ by the Mauritanian current (Figure 1). The in situ
 221 values of θ , S, SiO_4H_4 and NO from the rosette sampler profiles collected during the
 222 cruise were used to calculate the contribution of each WT to every sample, by solving
 223 this set of mass balance equations per sample:

$$\begin{aligned}
 224 & \\
 225 & \sum_i X_{ij} \cdot \theta_i = \theta_j + R\theta_j \\
 226 & \sum_i X_{ij} \cdot S_i = S_j + RS_j \\
 227 & \sum_i X_{ij} \cdot (\text{SiO}_4\text{H}_4)_i = (\text{SiO}_4\text{H}_4)_j + R(\text{SiO}_4\text{H}_4)_j \\
 228 & \sum_i X_{ij} \cdot \text{NO}_i = \text{NO}_j + R\text{NO}_j \\
 229 & \sum_i X_{ij} = 1 + R\Sigma
 \end{aligned}$$

230
 231 Where the subscript i corresponds to each WT and j to every sample; X_{ij} are the
 232 proportion of water type i in sample j; θ_i , S_i , $(\text{SiO}_4\text{H}_4)_i$ and NO_i are the WT i values of θ ,
 233 S, SiO_4H_4 and NO; and θ_j , S_j , $(\text{SiO}_4\text{H}_4)_j$ and NO_j are the values for each variable in
 234 sample j; R are the residuals each the mass balance equations and for the mass
 235 conservation equation for sample j.

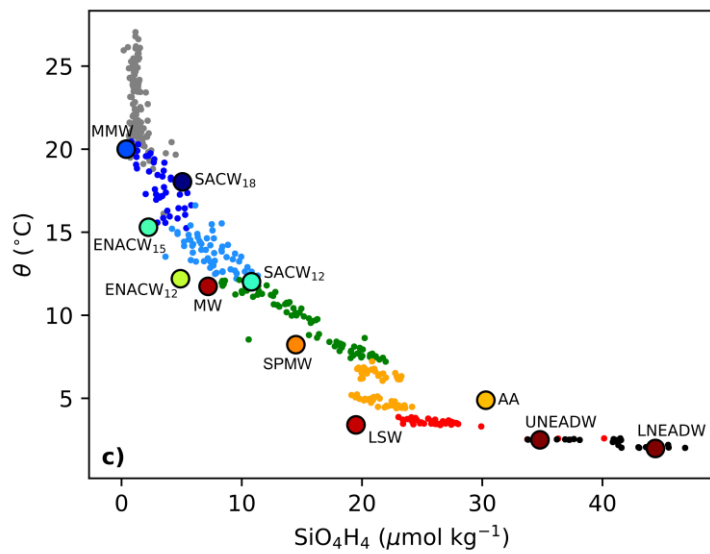
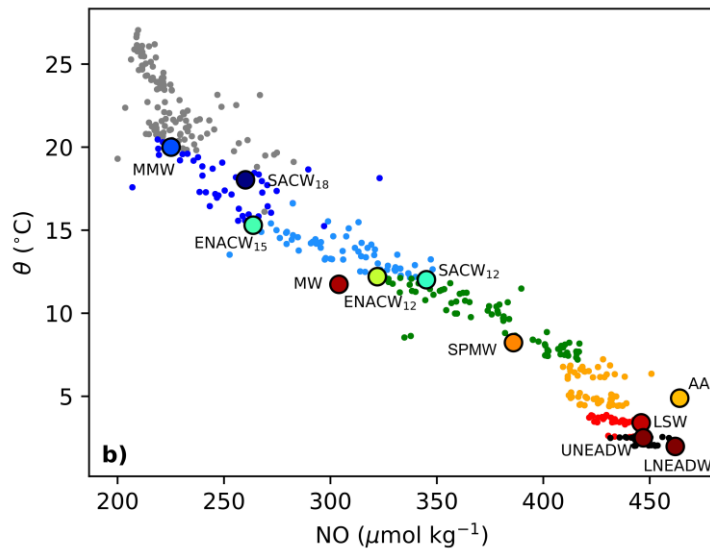
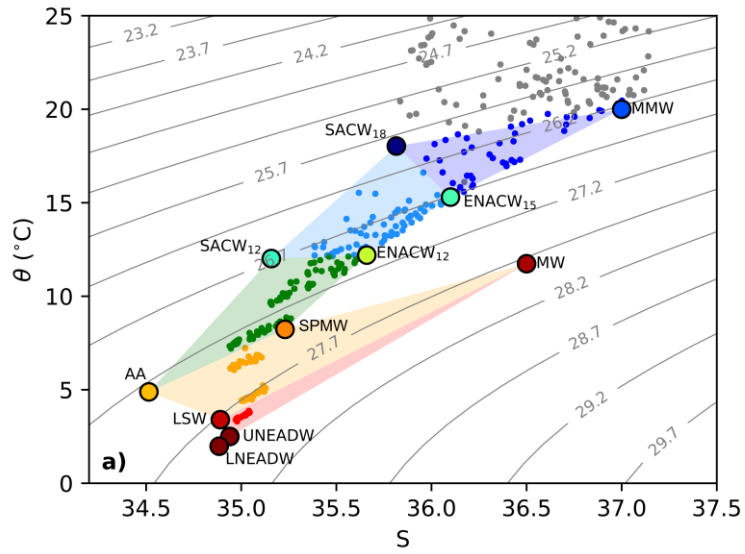
236

237 These linear mixing equations were normalized and weighted. For normalization,
238 the mean and standard deviation values of the parameters in Table 1 were used. The
239 equations were weighted considering the measurement error of each parameter in
240 relation to its variability in the study area and its relative conservative nature. Weights
241 of 10, 10, 2 and 1 were assigned to θ , S, NO and SiO_4H_4 , respectively. The weights
242 assigned to the NO and SiO_4H_4 mass balance equations were lower because both
243 variables are affected by non conservative processes: SiO_4H_4 is influenced by silica
244 dissolution and the R_N of NO is variable, which introduces more uncertainty in the mass
245 balance equations. We assumed that the mass is accurately conserved, so a weight of
246 100 was assigned to the mass conservation equation.

247
248 Since we have 5 mass balance equations and 11 WTs, in order to solve the OMP it
249 is necessary to define oceanographically consistent WT mixing groups, taking into
250 account that mixing occurs with adjacent WTs along or across isopycnals and a
251 maximum of 4 WTs can mix simultaneously (Álvarez et al., 2014). The 5 groups of
252 WTs defined, from surface to 4000 db were: 1) MMW - SACW18 - ENACW15; 2)
253 SACW18 - ENACW15 - SACW12 - ENACW12; 3) SACW12 - ENACW12 - SPMW -
254 AA; 4) SPMW - AA - MW - LSW; and 5) MW - LSW - LNEADW - UNEADW
255 (Figure 2). Each sample was assigned to a particular group according to its θ and S, and
256 then the system of mass balance equations was solved for each sample.

257
258 The reliability of the OMP analysis was assessed with the determination
259 coefficient (R^2) and standard error (SE) of the residuals of the linear regression between
260 measured and back-calculated variables (θ , S, SiO_4H_4 and NO) (Álvarez et al., 2014).
261 Note that our OMP reproduced the thermohaline and chemical fields during the cruise
262 quite accurately, as demonstrated by the high R^2 (>0.977) and low SE of the linear
263 regression of the measured and predicted values of θ , S, SiO_4H_4 and NO (Table 1).

264
265 Samples located between the surface and the base of the deep chlorophyll
266 maximum (DCM) were excluded from the OMP analysis because the heat, freshwater
267 and gas exchange with the atmosphere and the non conservative behaviour of O_2 and
268 nutrient salts would disprove the assumption of conservation of the mass balance
269 equations. Therefore, the OMP was applied to 307 of the 419 samples in which DOC,
270 DON, PON and POC were determined.



271

272 Figure 2. Potential temperature (θ) versus salinity (a), NO (b) and SiO_4H_4 (c) for FLUXES I. Dots
 273 represent the water samples collected and the shading colours in (a) identify the mixing group assigned to
 274 each sample. Potential density contours are also shown in (a).

275 Table 1. Thermohaline and chemical characteristics (average value \pm uncertainty) of the water types (WT)
 276 introduced in the OMP analysis of the water masses present in the CVFZ. Determination coefficient (R^2),
 277 standard error (SE) of the estimate and number of samples (n) of the multiple-regression of the measured
 278 and back-calculated variables.

WT	θ_i (°C)	S_i	SiO ₄ H _{4i} ($\mu\text{mol kg}^{-1}$)	NO _i ($\mu\text{mol kg}^{-1}$)
SACW_18 ^a	18.03 \pm 0.05	35.82 \pm 0.03	5.1 \pm 0.1	260 \pm 8
MMW ^b	20.0 \pm 0.5	37.00 \pm 0.04	0.4 \pm 0.3	225 \pm 10
ENACW_15 ^b	15.3 \pm 0.4	36.10 \pm 0.02	2.2 \pm 1.7	264 \pm 8
SACW_12 ^a	12.0 \pm 0.1	35.16 \pm 0.01	10.8 \pm 0.1	345 \pm 7
ENACW_12 ^c	12.2 \pm 0.4	35.66 \pm 0.02	4.9 \pm 0.2	322 \pm 8
SPMW ^c	8.2 \pm 0.4	35.23 \pm 0.01	14.5 \pm 0.4	386 \pm 7
AA ^a	4.89 \pm 0.03	34.51 \pm 0.02	30.3 \pm 0.8	464 \pm 8
MW ^c	11.8 \pm 0.1	36.50 \pm 0.01	7.2 \pm 0.7	304 \pm 9
LSW ^c	3.4 \pm 0.2	34.89 \pm 0.12	19.5 \pm 0.4	446 \pm 9
UNEADW ^d	2.500 \pm 0.003	34.940 \pm 0.003	34.8 \pm 0.3	447 \pm 7
LNEADW ^d	1.980 \pm 0.002	34.884 \pm 0.003	44.4 \pm 0.3	462 \pm 7
R ²	0.999	0.999	0.988	0.977
SE	0.04	0.005	1.2	11
N	307	307	307	307

^a This work, taken from the WOA13 in the Equatorial Atlantic

^b Álvarez and Álvarez-Salgado (2009); Lonborg & Álvarez-Salgado (2014)

^c Perez et al. (2001); Álvarez and Álvarez-Salgado (2009)

^d Perez et al. (2001); Lonborg & Álvarez-Salgado (2014)

279

280 2.4. WT proportion-weighted average values

281 The WT proportion-weighted average value of any variable (N) in a given WT,
 282 henceforward archetype concentration of N , can be calculated using the X_{ij} obtained as
 283 detailed in section 2.3, and the concentration of N in each sample (Álvarez-Salgado et
 284 al., 2013). The equation is:

285

$$N_i = \frac{\sum_j X_{ij} \cdot N_j}{\sum_j X_{ij}}$$

287

288 Where N_i is the archetype value of N in water mass i ; X_{ij} is the proportion of WT i in
 289 sample j and N_j is the value of N in sample j . The standard error of the archetype value
 290 is obtained as:

291

$$SE_{N_i} = \frac{\sqrt{\sum_j X_{ij} (N_j - N_i)^2}}{\sum_j X_{ij}}$$

292

293

294 Finally, the proportion of the total volume of water sampled during the cruise that
295 correspond to a given water mass (%VOL_{*i*}) can be calculated as:

296

$$297 \quad \%VOL_i = 100 \cdot \frac{\sum_j X_{ij}}{n}$$

298

299 Where *n* is number of samples. In this study, we have calculated archetype values
300 of Z, S, θ, AOU, DOC, DON, POC and PON for the 11 WTs identified in the study
301 area. Moreover, *N_i* values were calculated also for the Northern (stns 3 to 12, excluding
302 stations 1 and 2 over the continental shelf) and Southern transects (stns 19 to 29) -
303 separated by the CVF- and the Western transect (stns 12 to 19) -located in the open
304 ocean- and the Eastern transect (stns 29 to 35 and stn 3) near the coast (Figure 1), to
305 assess geographical differences between transects within a given WT.

306

307 2.5. Multiple regression models

308 The fraction of the total variability of the distribution of a non-conservative
309 variable (e.g. DOC, DON, POC, PON) explained by WT mixing can be calculated from
310 a multiple linear regression of the non-conservative variable with the water mass
311 proportions:

$$312 \quad N_j = \sum_j X_{ij} \cdot n_i$$

313 Where *N_j* is the concentration of the non-conservative variable, with *j* = 1... *n* (one per
314 sample) and *n_i* is the correlation coefficient of WT *i*, with *i* = 1... *m* (one per WT). The
315 per cent of explained variability is indicated by the determination coefficient (*R*²) and
316 the explanatory power by the standard error of the estimate (SE) of the multiple
317 regression.

318

319 However, the distributions of DOC, DON, POC or PON depend not only on the
320 conservative mixing of WTs but also on the biogeochemical processes that occur
321 alongside mixing. The main biogeochemical process in the ocean interior is organic
322 matter mineralisation and it can be traced with AOU (Álvarez et al., 2014). The
323 observed organic matter mineralisation is the result of the large-scale mineralisation
324 from the formation area of each WT to the study area and the local mineralisation that

occurs within the study area (Álvarez-Salgado et al., 2013; Álvarez et al., 2014), the CVFZ in our case. On the one hand, the large-scale mineralisation is assumed to be included in the archetype value of each WT and, therefore, accounted for by the multiple linear regression with X_{ij} . On the other hand, a multiple linear regression with X_{ij} and AOU (for DOC, DON, POC and PON) or NO_3^- (for DON and PON) would quantify the local mineralisation of DOM and suspended POM:

$$N_j = \sum_j X_{ij} \cdot n_i + \beta \cdot \text{AOU (or } \text{NO}_3^-)$$

In this multiple linear regression of n linear equations with $m + 1$ unknowns, the extra unknown (β) is the coefficient that relates DOC, DON, POC or PON with AOU or NO_3^- and represents the rate of change of DOM and suspended POM with AOU or NO_3^- that does not depend on WT mixing (Álvarez-Salgado et al., 2013). Therefore, when calculating the multiple linear regression of DON or PON with X_{ij} and NO_3^- , the coefficient β would represent the contribution of DON or PON to the local NO_3^- production by organic matter mineralisation. On the other hand, the coefficient β in the multiple linear regression of DOC or POC to AOU would represent the contribution of DOC or POC to the oxygen utilisation. In this case, once β is multiplied by the Redfield ratio of dissolved oxygen consumption to organic carbon mineralisation of 1.4 mol O_2 mol C^{-1} (Anderson, 1995), it would represent the contribution of DOC or POC to the local production of inorganic nitrogen by organic matter mineralisation. Finally, once the contribution of DOM and suspended POM to organic matter mineralisation is calculated from β , the contribution of sinking POM can be estimated indirectly by difference.

2.6. Epipelagic layer

As indicated above, samples collected in the epipelagic layer were excluded from the OMP analysis because of the non-conservative behaviour of θ , S, SiO_4H_4 and NO. Those samples have been used to study the impact of the CVFZ on the biogeochemistry of the epipelagic layer during the FLUXES I cruise. To do that, we have calculated average concentrations of the different variables (Z, S, θ , AOU, Chl-a, NO_2^- , NO_3^- , NH_4^+ , DOC, DON, POC and PON) at the surface (5 db), and the deep chlorophyll maximum (DCM), as well as vertically-averaged from the surface to the base of the DCM. Vertical averages considered the uneven vertical sampling spacing by using the

358 trapezoid rule to weight each sample. The average values were obtained for the whole
359 cruise as well as for each individual transect. In the Northern transect, the first two
360 stations were excluded because they are outside the box, and due to their position close
361 to the continental shelf, they are affected by distinct processes from those observed in
362 the oceanic waters, biasing the calculation of the average values of the Northern transect
363 (Figure 1).

364

365 **3. Results**

366 **3.1. Hydrographic setting of the CVFZ**

367 **3.1.1 Epipelagic waters**

368 The relative position of the four transects with respect to the CVF during
369 FLUXES I can be documented using the isohaline that defines the front (36 at 150 db)
370 (Zenk et al., 1991) (Figure 3a). According to this criterion, the Western and Northern
371 transects were located to the North of the front, while the front intersected the Southern
372 and Eastern transects around stations 34 and 24, respectively (Figure 1). Due to the
373 dominance of saline waters of North Atlantic origin to the North of the front, the
374 average salinity was significantly higher in the Northern and Western transects (36.7-
375 36.8), than in the Southern and Eastern transects (36.2) (Figure 3a, Table S1).
376 Mesoscale variability was super-imposed over this large-scale pattern, notably due to
377 the presence of a narrow intrusion of relatively cold and less saline water of South
378 Atlantic origin centred at stn 5 in the Northern transect. The mean depth-averaged
379 temperature down to the base of the DCM was 22.3°C with non-significant differences
380 between transects (Figure 3b, Table S1). Nonetheless, the Southern transect was
381 characterized by significantly higher ($p < 0.0005$) surface (5 db) temperatures (26.1°C)
382 than the Northern transect (23.9°C).

383

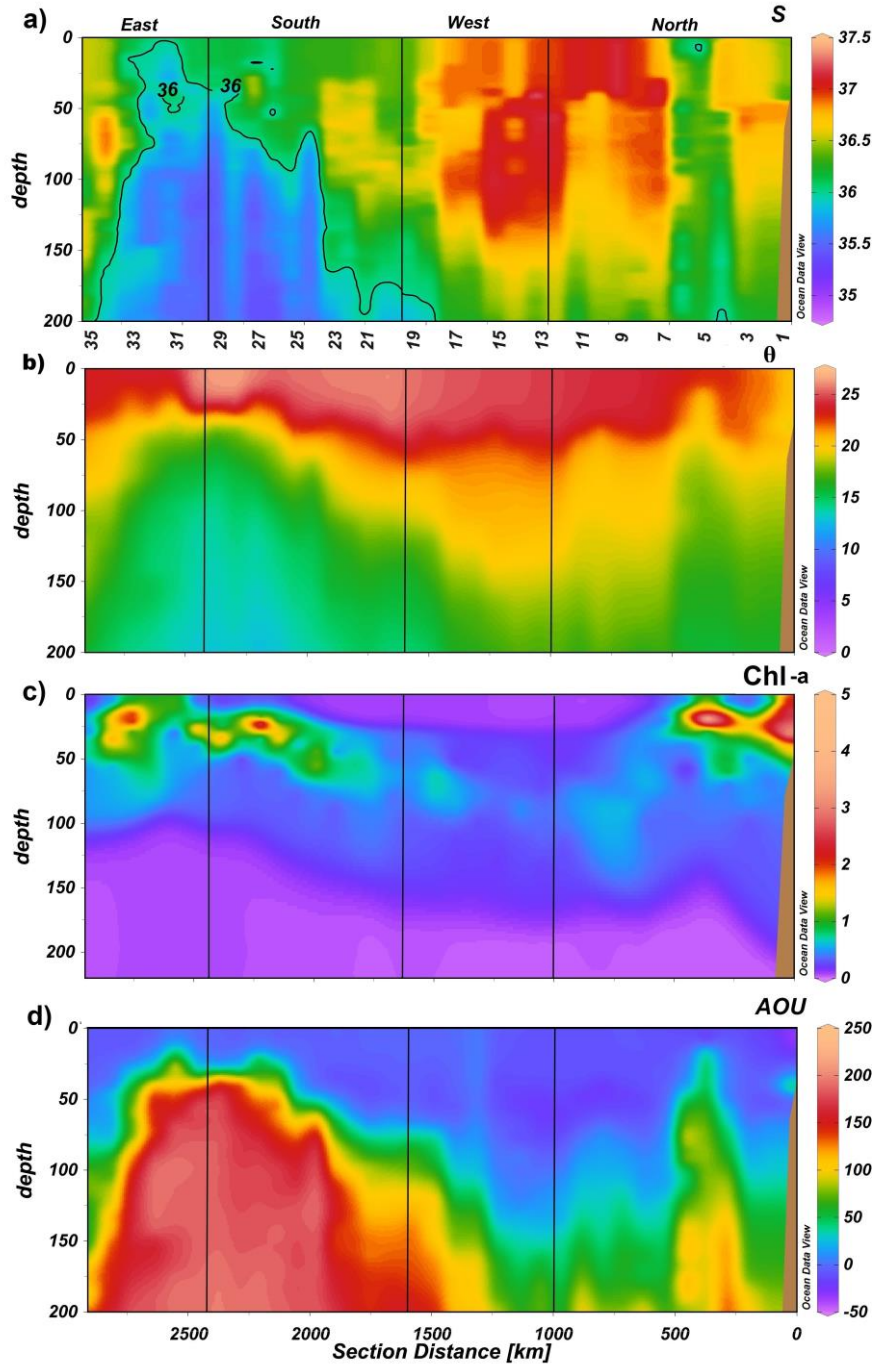
384 The DCM was shallower and with higher Chl-a levels towards the coast (Figure
385 3c). The average depth of the DCM and average Chl-a levels in the Northern and
386 Southern transect, were similar ($p > 0.3$) while the Western (oceanic) and Eastern
387 (coastal) transects showed the highest differences, being the DCM deeper and with
388 lower concentrations in the Western transect (Table S1).

389

1
2
3
4
5
6
7
8
9
10
11
12
13
14
15
16
17
18
19
20
21
22
23
24
25
26
27
28
29
30
31
32
33
34
35
36
37
38
39
40
41
42
43
44
45
46
47
48
49
50
51
52
53
54
55
56
57
58
59
60
61
62
63
64
65

390 The distribution of AOU (Figure 3d) matched the predominant form of inorganic
391 nitrogen, NO_3^- (Figure 4a), increasing significantly with depth (Table S1). In the same
392 way as salinity and temperature, marked differences were observed between the
393 Northern and Southern transects of the CVF: depth-averaged concentrations of AOU
394 and NO_3^- were significantly lower ($p < 0.05$) in the Northern and Western transects
395 (<4.5 and $<2.3 \mu\text{mol kg}^{-1}$, AOU and NO_3^- respectively) than in the Southern and Eastern
396 transects (>20 and $>4.6 \mu\text{mol kg}^{-1}$, respectively). The intrusion of water with South
397 Atlantic origin at stn 5 is traced by higher AOU and NO_3^- values in the upper 100 db
398 (Figures 3d, 4a).

399
400 NH_4^+ (Figure 4b) and NO_2^- (Figure 4c) were, in general, very low (<0.06 and
401 $<0.14 \mu\text{mol kg}^{-1}$), except in the surroundings of the DCM. An average NH_4^+
402 concentration of $0.09 \pm 0.03 \mu\text{mol kg}^{-1}$ was observed at the DCM, with significantly (p
403 < 0.01) lower values ($0.02 \pm 0.03 \mu\text{mol kg}^{-1}$) in the Western (oceanic) transect and
404 higher values ($0.19 \pm 0.10 \mu\text{mol kg}^{-1}$) in the Eastern (coastal) transect. The average
405 concentration of NO_2^- at the DCM was $0.23 \pm 0.03 \mu\text{mol kg}^{-1}$, being also significantly
406 lower in the Western transect ($p < 0.025$).

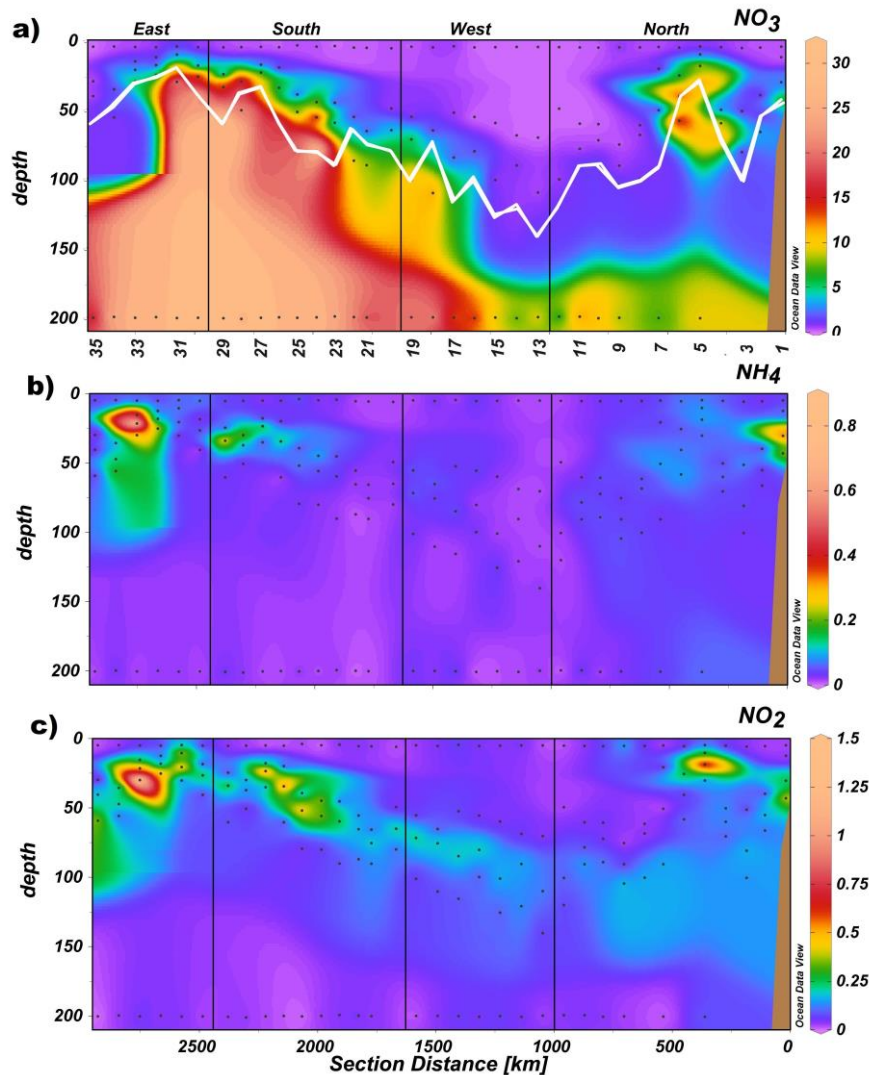


408

409 Figure 3. Distribution of salinity (S) (a), potential temperature (θ) in $^{\circ}\text{C}$ (b), Chl (chlorophyll a) in $\mu\text{g L}^{-1}$
 410 (c) and apparent oxygen utilization (AOU) in $\mu\text{mol kg}^{-1}$ (d), in the epipelagic layer during the FLUXES I
 411 cruise. The black line in (a) represents the 36 isohaline defining the location of the CVF, and the vertical
 412 black lines represent the corners of the FLUXES hydrographic box. The y-axis can be read as station
 413 number (a) or section distance (d). Produced with Ocean Data View (Schlitzer, 2017).

414 NH_4^+ and NO_2^- also showed relatively elevated concentrations at stn 5 in the
 415 Northern transect, coinciding with the relative maxima in temperature, Chl-a, AOU and
 416 NO_3^- , and minimum in salinity, reflecting the influence of the mesoscale variability of
 417 the CVF in the distribution of biogeochemical properties.

418



419

420 Figure 4. Distributions of nitrate (NO_3^-) in $\mu\text{mol kg}^{-1}$ (d) (a), ammonium (NH_4^+) in $\mu\text{mol kg}^{-1}$ (b), and
 421 nitrite (NO_2^-) in $\mu\text{mol kg}^{-1}$ (c), in the epipelagic layer during the FLUXES I cruise. Dots represent
 422 samples, vertical back lines represent the corners of the FLUXES I hydrographic box and the white line in
 423 panel a represents the base of the DCM. The y-axis can be read as station number (a) or section distance
 424 (c). Produced with Ocean Data View (Schlitzer, 2017).

425 3.1.2. Meso- and bathypelagic waters

426 Below the epipelagic layer, in the depth range between 100-700 db, hydrographic
 427 variability was governed by the distribution of the central water types. SACW_18 and
 428 MMW, characterized by potential temperatures of 18°C and 20°C , respectively (Table 1,
 429 Figures 5ab, S1a), and centred at about 110 db (Table 2) were the shallowest central
 430 water types. SACW_18 and MMW were defined by distinct salinity values, 35.82 and
 431 37.00, respectively (Table 1, Figures 5ab, S1b), as expected for two water masses of
 432 contrasting North and South Atlantic origin, and represented 4.78% and 5.48% of the
 433 total sampled water volume (Table 2) or 9.9% and 11.4% of the volume of central waters.
 434 ENACW_15 was located deeper, centred at 240 ± 14 db (Table 2) and represented

1
2
3
4
5
6
7
8
9
10
11
12
13
14
15
16
17
18
19
20
21
22
23
24
25
26
27
28
29
30
31
32
33
34
35
36
37
38
39
40
41
42
43
44
45
46
47
48
49
50
51
52
53
54
55
56
57
58
59
60
61
62
63
64
65

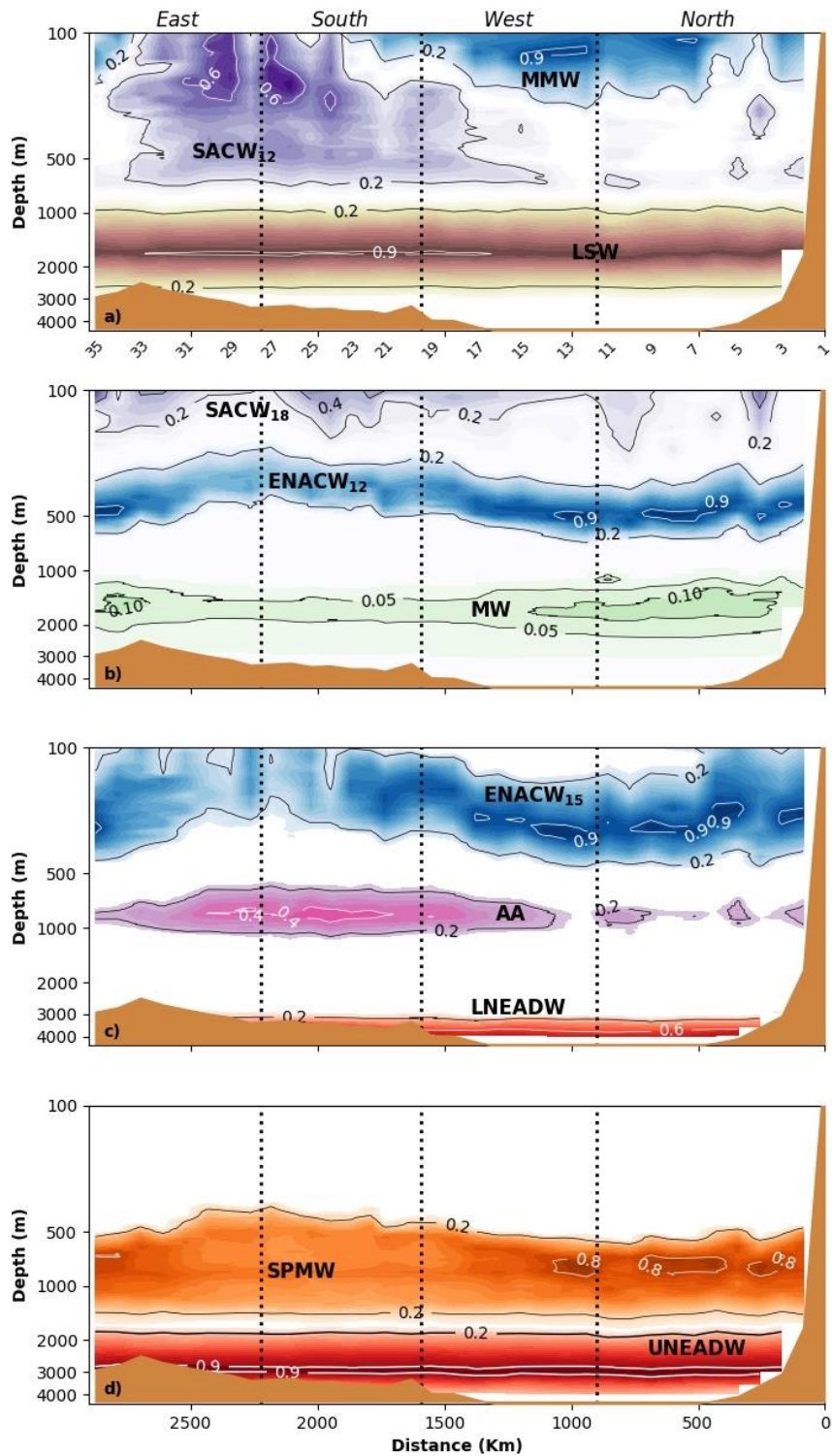
435 12.54% of the total sampled volume or 26.1% of the volume of central waters. Most of
436 the ENACW_15 was present in the Northern and Western transects (42.8% and 25.0%
437 of the volume of this WT, respectively), i.e. to the North of the CVF (Figure 5c).
438 SACW_12 and ENACW_12 were centred at 336 ± 28 db and 442 ± 19 db and were
439 defined by a similar temperature of $\sim 12^\circ\text{C}$, but different values of salinity (35.16 and
440 35.66), SiO_4H_4 (10.8 and $4.9 \mu\text{mol kg}^{-1}$) and NO (345 and $322 \mu\text{mol kg}^{-1}$) (Table 1).
441 ENACW_12 was the most abundant WT sampled during the cruise with 18.09% (Table
442 2, Figure 5b) or 37.6% of the volume of central waters and was present in the four
443 transects (from a minimum of 17.8% of the total volume in the Western transect to a
444 maximum of 28.6% in the Northern transect). Conversely, SACW_12 occupied a
445 volume of 7.25% (or 15.1% of the central waters) and was mostly present in the stations
446 of the Southern transect, where 57% of the volume of this WT was found (Table 2,
447 Figure 5a). Again, in the Northern section, around stn 5, SACW_18 appears, although
448 ENACW dominated in the rest of the transect (Figure 5).

449

450 The intermediate water domain, approximately between 700 db and 1500 db, was
451 occupied by AA, SPMW and MW. These water masses, of contrasting sub-Antarctic,
452 sub-Arctic and Mediterranean origin, have remarkable differences in θ , S, SiO_4H_4 and
453 NO (Table 1). It is particularly noticeable the salinity minimum observed in the
454 Southern transect at about 1000 db, which corresponds to AA (Figures 5c, S1b). The
455 shallowest intermediate WT was the SPMW, centred at 809 ± 32 db, with a temperature
456 of 8°C and representing 7.18% of the sampled volume (or 34.3% of the intermediate
457 waters).

458

459 SPWM was followed by AA at a depth of 873 ± 54 db, which had the lowest
460 salinity 34.52 but the highest content of silicates $30.3 \mu\text{mol kg}^{-1}$ and occupied a volume
461 of 10.62% (or 50.8% of the intermediate waters). This water mass was mostly present to
462 the South of the CVF (59.0% of the volume sampled in the Northern and Western
463 transects) while SPMW predominated to the North of the front (56.8% of the sampled
464 volume in the Eastern and Southern transects) (Figure 5d). The deepest intermediate
465 WT, MW, centred at 1455 ± 118 db, was much less represented with 3.09% (14.8% of
466 the intermediate waters) and was almost absent in the Eastern transect (only 3.1% of the
467 volume).



468

469 Figure 5. Distributions of the water masses described in the CVFZ during the FLUXES I cruise. Vertical
 470 black lines represent the corners of the FLUXES I hydrographic box. Water mass proportions in this
 471 figure were derived with an OMP analysis applied to CTD data at 1 db vertical resolution. θ and S were
 472 measured directly with the CTD, while SiO_4H_4 and NO values were reconstructed by fitting the measured
 473 water sample concentrations to a non-linear combination of variables directly measured with the CTD (θ ,
 474 S , O_2) (Figures S1 and S2). The distribution of the water-masses among the panels was designed to avoid
 475 contour overlapping and does not follow an oceanographic criteria. The y-axis can be read as station
 476 number (a) or section distance in km (d).

477 Table 2. Percentage of the total volume of water sampled during FLUXES I that corresponded to each
 478 water type (%VOLi) and archetype values \pm SE of depth (Zi), apparent oxygen utilization (AOUi), nitrate
 479 (NO_3^- i), dissolved organic carbon (DOCi), dissolved organic nitrogen (DONi), particulate organic carbon
 480 (POCi), particulate organic nitrogen (PONi), and C:N ratios of DOM and suspended POM for the water
 481 types intercepted during the cruise. Determination coefficient (R^2), standard error of the estimate (SE) of
 482 the multiple-regression of each variable with the water type proportions X_{ij} .

WT	%VOLi	Zi (db)	AOUi ($\mu\text{mol kg}^{-1}$)	NO_3^- i ($\mu\text{mol kg}^{-1}$)	DOCi ($\mu\text{mol L}^{-1}$)	DONi ($\mu\text{mol L}^{-1}$)
SACW_18	4.78%	102 \pm 19	120.2 \pm 15.4	16.9 \pm 2.1	58.9 \pm 2.5	4.6 \pm 0.4
MMW	5.48%	113 \pm 3	50.9 \pm 10.5	6.5 \pm 1.4	58.7 \pm 1.6	5.1 \pm 0.3
ENACW_15	12.54%	240 \pm 14	117.8 \pm 6.7	16.2 \pm 1.0	52.3 \pm 1.7	4.2 \pm 0.3
SACW_12	7.25%	336 \pm 28	191.7 \pm 5.4	28.7 \pm 1.0	49.9 \pm 1.5	3.5 \pm 0.3
ENACW_12	18.09%	442 \pm 19	171.2 \pm 4.8	27.2 \pm 0.8	48.5 \pm 0.6	3.4 \pm 0.2
SPMW	7.18%	809 \pm 32	175.7 \pm 4.2	30.9 \pm 0.7	44.8 \pm 0.6	3.3 \pm 0.3
AA	10.62%	873 \pm 54	172.6 \pm 5.7	31.3 \pm 0.6	45.1 \pm 0.6	3.1 \pm 0.3
MW	3.09%	1455 \pm 118	119.4 \pm 9.2	25.9 \pm 1.2	43.3 \pm 0.9	3.0 \pm 0.4
LSW	15.58%	1688 \pm 46	104.0 \pm 2.6	23.9 \pm 0.3	43.4 \pm 0.5	3.0 \pm 0.2
UNEADW	11.72%	2742 \pm 93	88.0 \pm 1.1	22.2 \pm 0.2	43.4 \pm 0.6	2.9 \pm 0.2
LNEADW	3.66%	3824 \pm 101	85.1 \pm 1.7	22.4 \pm 0.2	43.5 \pm 1	3.1 \pm 0.3
R^2			0.94	0.95	0.63	0.44
SE			12.9	1.8	4.0	0.9

483

484

485

WT	POCi ($\mu\text{mol L}^{-1}$)	PONi ($\mu\text{mol L}^{-1}$)	C:N DOM (mol C mol N ⁻¹)	C:N POM (mol C mol N ⁻¹)
SACW_18	3.2 \pm 1.2	0.33 \pm 0.13	12.7 \pm 1.1	9.9 \pm 1.6
MMW	2.7 \pm 1.0	0.25 \pm 0.10	11.6 \pm 0.7	10.9 \pm 1.3
ENACW_15	1.5 \pm 0.3	0.12 \pm 0.03	12.4 \pm 1.0	12.3 \pm 0.9
SACW_12	1.4 \pm 0.2	0.11 \pm 0.02	14.4 \pm 1.5	12.4 \pm 1.4
ENACW_12	1.2 \pm 0.1	0.09 \pm 0.01	14.4 \pm 1.1	12.5 \pm 0.8
SPMW	0.79 \pm 0.06	0.05 \pm 0.01	13.6 \pm 1.3	14.5 \pm 1.3
AA	0.81 \pm 0.06	0.06 \pm 0.01	14.6 \pm 1.3	14.2 \pm 1.3
MW	0.70 \pm 0.11	0.05 \pm 0.01	14.4 \pm 1.9	14.2 \pm 2.2
LSW	0.67 \pm 0.05	0.05 \pm 0.01	14.5 \pm 0.9	14.6 \pm 1.1
UNEADW	0.68 \pm 0.07	0.04 \pm 0.01	15.2 \pm 0.9	15.6 \pm 1.3
LNEADW	0.71 \pm 0.12	0.04 \pm 0.01	14.8 \pm 1.5	17.3 \pm 2.0
R^2	0.26	0.29		
SE	1.3	0.13		

486 Finally, the deep waters domain was composed by three water types with similar
 487 salinity, yet different silicate content (Figure S1c) due to their contrasting origin. While
 488 LSW is of pure North Atlantic origin, LNEADW and UNEADW are mixed with
 489 Antarctic waters that confer their higher silicate concentration. LSW was defined by a

1
2
3
4
5
6
7
8
9
10
11
12
13
14
15
16
17
18
19
20
21
22
23
24
25
26
27
28
29
30
31
32
33
34
35
36
37
38
39
40
41
42
43
44
45
46
47
48
49
50
51
52
53
54
55
56
57
58
59
60
61
62
63
64
65

490 silicate concentration of $19.5 \mu\text{mol kg}^{-1}$, it was located at 1648 ± 46 db and represented
491 15.58% of the sampled volume (50.3% of the deep waters), being the second
492 predominant water mass sampled during FLUXES I. LSW was found in the four
493 transects, ranging from 19.9% of the total volume in the Eastern transect to 29.4% in the
494 Northern transect (Figure 5a). In contrast, UNEADW was located deeper at 2742 ± 93
495 db and had a silicate concentration of $34.8 \mu\text{mol kg}^{-1}$, with a volume sampled of 11.72%
496 (37.9% of the deep waters). LNEADW was placed at 3824 ± 101 db, with a silicate
497 concentration of $44.4 \mu\text{mol kg}^{-1}$ and a small representation of sampled volume of 3.66%
498 (or 11.8% of deep waters). UNEADW was distributed in the four transects, ranging
499 from 18.7% of the total volume in the Eastern transect to 29.0% in the Southern transect
500 (Figure 5d). In contrast, LNEADW concentrated in the Northern and Western transects
501 (75% of the total volume of this WT) while it was practically absent in the Eastern
502 transect. Bottom depth is the likely reason behind this difference (Figure 5c).

503 504 **3.2. Biogeochemical variability in epipelagic, meso- and bathypelagic waters** 505 **of the CVFZ**

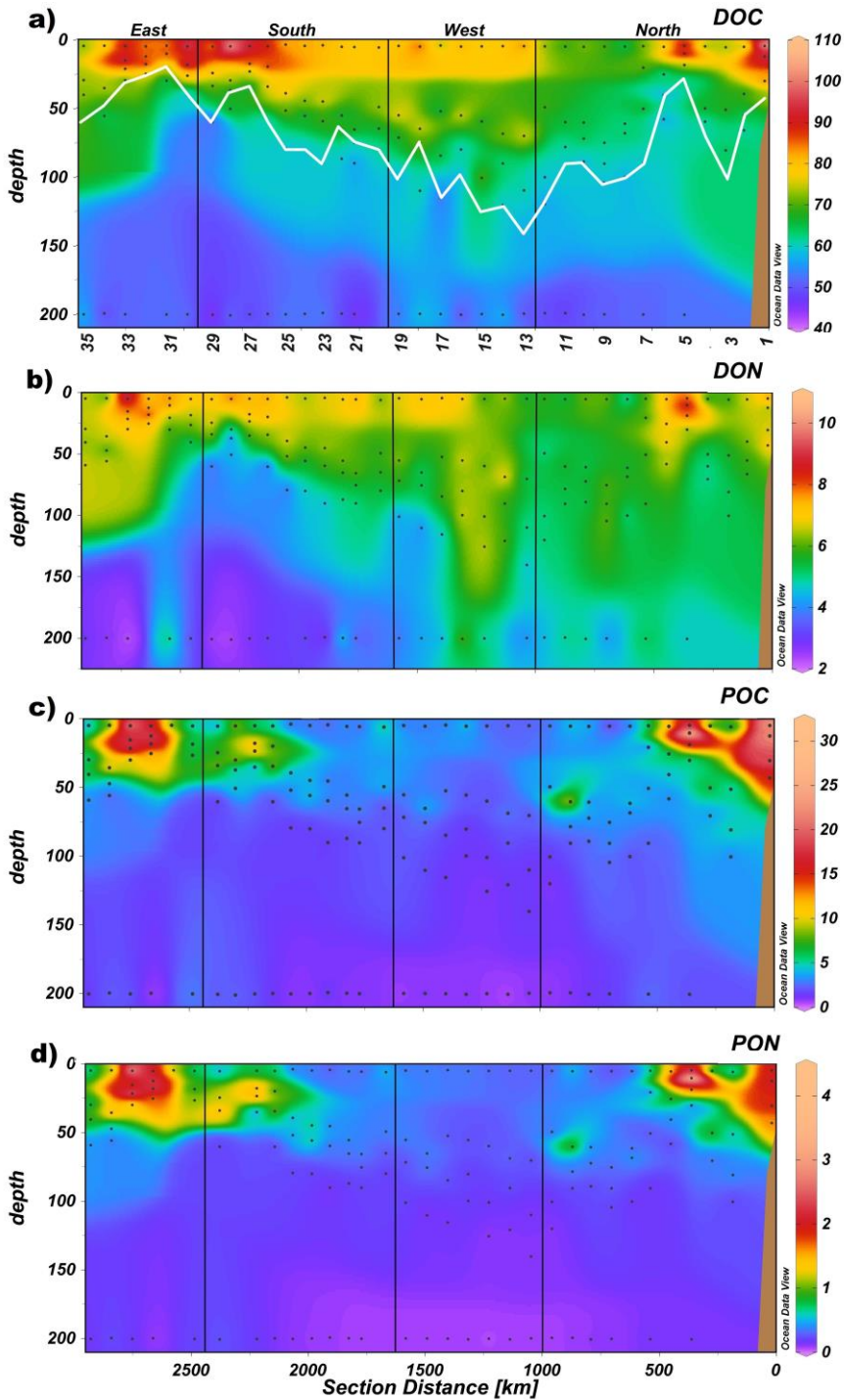
506 **3.2.1 Organic matter variability in epipelagic waters**

507 DOC (Figure 6a) and DON (Figure 6b) showed maximum average concentrations
508 of $80.9 \pm 1.7 \mu\text{mol L}^{-1}$ and $6.7 \pm 0.2 \mu\text{mol L}^{-1}$ at the surface layer (Table S1), and
509 decreased with depth. At the surface, DOC and DON levels were significantly higher in
510 the Southern transect, while at the DCM, the highest DOC and DON concentrations
511 were found in the Eastern (coastal) transect (Table S1, Figure 6a,b). The average C:N
512 molar ratio of DOM throughout the epipelagic layer was 12.0 ± 0.3 and showed similar
513 values in all transects at the surface and the DCM ($p > 0.05$).

514
515 POC (Figure 6c) and PON (Figure 6d) concentrations showed similar distributions
516 with a marked decrease below the DCM. Maximum concentrations of POC and PON
517 were observed at the stations near the coast, in the Northern and Eastern transects.

518
519 Maximum POC coincided with the DCM in the Eastern ($10.4 \pm 2.0 \mu\text{mol L}^{-1}$)
520 transect, in the Western ($2.8 \pm 0.3 \mu\text{mol L}^{-1}$) transect it was located at the surface, while
521 in the Northern ($6.9 \pm 2.1 \mu\text{mol L}^{-1}$) and Southern ($5.7 \pm 1.1 \mu\text{mol L}^{-1}$) transects it was
522 somewhat above the DCM. Maximum PON concentrations followed the same pattern

523 (Figure 6d). In the upper 50 db, stn 5 shows very high values of DOC, DON, POC and
 524 PON.



525
 526 Figure 6. Distributions of DOC in $\mu\text{mol L}^{-1}$ (a), DON in $\mu\text{mol L}^{-1}$ (b), POC in $\mu\text{mol L}^{-1}$ (c) and
 527 PON in $\mu\text{mol L}^{-1}$ (d) in the epipelagic layer during the FLUXES I cruise, dots represent samples, vertical
 528 black lines represent the corners of the FLUXES I hydrographic box, and the white line in a) represent the
 529 base of DCM. The y-axis can be read as station number (a) or section distance in km (d). Produced with
 530 Ocean Data View (Schlitzer, 2017).

531 The average value of the C:N molar ratio of POM over the epipelagic layer, 8.1
532 ± 0.4 , was significantly lower than the average C:N molar ratio of DOM, 12.0 ± 0.3
533 (Table S1). Average C:N ratios of POM were significantly higher in the Northern and
534 Western transects (>8.9) than in the Southern and Eastern transects (<7.3) ($p < 0.005$).
535 In the Western, Southern and Eastern transects, minimum values of the C:N ratio of
536 POM were associated with the DCM as for the case of the C:N ratio of DOM (Table
537 S1).

538

539 **3.2.2 Organic matter variability in meso- and bathypelagic waters**

540 AOU can be used to trace organic matter mineralisation in the meso- and
541 bathypelagic layers of the CVFZ (Figure 7a). In the central waters, the lowest archetype
542 AOU values (50 to $120 \mu\text{mol kg}^{-1}$) were found in the shallowest WTs (MMW,
543 ENACW_15 and SACW_18), while the highest archetype AOU ($192 \mu\text{mol kg}^{-1}$)
544 corresponded to SACW_12 (Table 2). In intermediate and deep waters, AOU decreased
545 significantly ($p < 0.0005$) with depth from an archetype value of $176 \mu\text{mol kg}^{-1}$ in
546 SPMW to $85 \mu\text{mol kg}^{-1}$ in the LNEADW. WTs mixing explained 94% of the variability
547 of AOU, but the SE of $12.9 \mu\text{mol kg}^{-1}$ was larger than the measurement error of ~ 1
548 $\mu\text{mol kg}^{-1}$ (Table 2).

549

550 Regarding the geographical variability within WTs, ENACW_12, the only central
551 WT with significant presence in the four transects, showed significantly ($p < 0.01$)
552 lower AOU levels in the Northern transect ($144 \mu\text{mol kg}^{-1}$) and higher in the Southern
553 transect ($204 \mu\text{mol kg}^{-1}$; Table S2). In intermediate waters, AOU in SPMW and AA was
554 also significantly higher in the Southern transect ($p < 0.05$). In deep waters, archetype
555 AOU levels in LSW did not differ between transects, while in UNEADW, they were
556 significantly ($p < 0.025$) higher in the Southern and Eastern transects ($90\text{--}96 \mu\text{mol kg}^{-1}$)
557 as compared with the Northern and Western transects ($83 \mu\text{mol kg}^{-1}$).

558

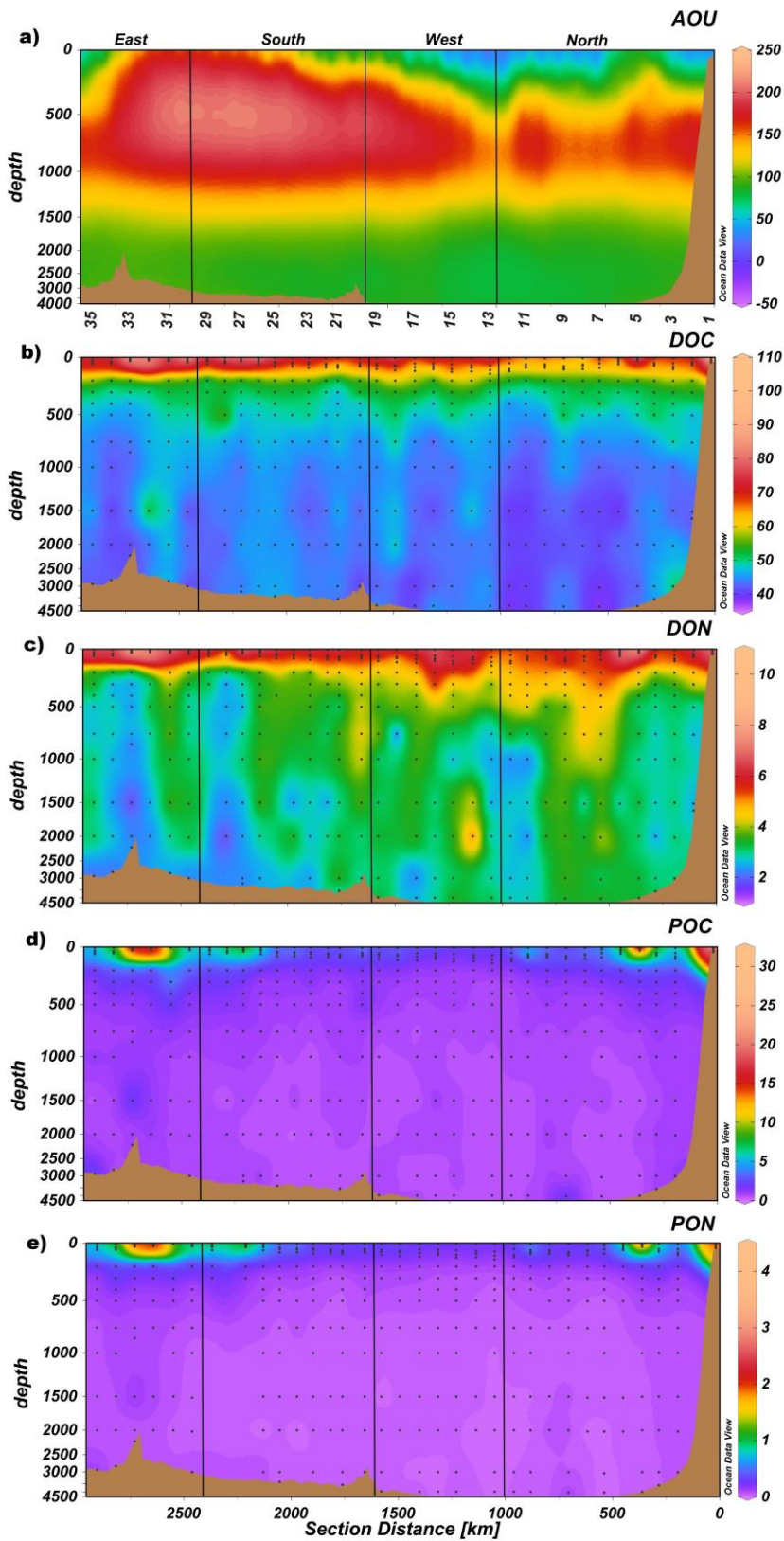
559 Archetype DOC values (Figure 7b) ranged from $58.9 \pm 2.5 \mu\text{mol L}^{-1}$ in SACW_18
560 to $43.4 \pm 0.6 \mu\text{mol L}^{-1}$ in LNEADW (Table 2). The multiple regression with X_{ij}
561 explained 63% of the DOC variability with a SE ($4.0 \mu\text{mol L}^{-1}$) that was about 3–4
562 times the measurement error of DOC. The addition of AOU to the multiple linear
563 regression increased the explained variability to 70% and produced a 15% reduction of
564 SE (Table 3). The AOU coefficient of the multiple regression, $-0.026 \pm 0.015 \text{ mol C}$

1
2
3
4
5
6
7
8
9
10
11
12
13
14
15
16
17
18
19
20
21
22
23
24
25
26
27
28
29
30
31
32
33
34
35
36
37
38
39
40
41
42
43
44
45
46
47
48
49
50
51
52
53
54
55
56
57
58
59
60
61
62
63
64
65

565 mol O₂⁻¹, represents the average stoichiometric ratio of DOC to O₂ consumption for the
566 meso- and bathypelagic waters in the CVFZ. This ratio is independent of water mass
567 mixing and indicates that DOC mineralisation may explain 3.6 ± 2.1% of the inorganic
568 carbon production in the area, assuming a -O₂:C Redfield ratio of 1.4 mol O₂ mol C⁻¹.
569 The AOU coefficient of the multiple linear regression of DOC with X_{ij} and AOU was
570 -0.061 ± 0.032 and -0.150 ± 0.038 mol C mol O₂⁻¹ for the Northern and Southern
571 transects, respectively. Therefore, although DOC represented only 3.6 ± 2.1 % of the
572 organic matter mineralised in the water masses of the CVFZ, it accounted for 9 ± 4 %
573 and as much as 21 ± 5% in the Northern and Southern transects, respectively (Table
574 S3).

575
576 DON (Figure 7c) decreased with depth from 5.1 ± 0.3 μmol L⁻¹ in MMW to 3.1 ±
577 0.3 μmol L⁻¹ in the deepest WT, LNEADW (Table 2). WTs mixing explained 44% of
578 the variability of the distribution of DON in the CVFZ with a SE of 0.90 μmol L⁻¹, 3
579 times the measurement error (Table 2). R² increased to 46% and SE reduced by 22%
580 when the multiple linear regression included X_{ij} and AOU as explanatory variables.
581 When NO₃⁻ was included as an explanatory variable, R² increased to 55% and SE
582 reduced by 19%. In this case, the NO₃⁻ coefficient of -0.16 ± 0.02 indicated that 16% of
583 nitrate is produced following DON mineralisation in the CVFZ, a larger fraction than
584 obtained for DOC and AOU (Table 3). When analysing the DON to NO₃⁻ coefficient of
585 the multiple linear regression with X_{ij} and NO₃⁻ transect by transect, we obtained
586 significant values only for the Northern (-0.12 ± 0.03) and Southern (-0.16 ± 0.03)
587 transects (Table S3).

588
589 POC (Figure 7d) decreased with depth down to the MW level and then remained
590 almost constant to the bottom. The highest concentrations of POC, 3.2 ± 1.2 and 2.7 ±
591 1.0 μmol L⁻¹, were found in the shallowest central waters SACW_18 and MMW,
592 respectively (Table 2). WTs mixing explained only 26% of the POC variability in the
593 CVFZ (Table 2), which increased to 38% when AOU was included in the multiple
594 linear regression, accompanied by a SE reduction of 46% (Table 3). The AOU
595 regression coefficient was -0.032 ± 0.005 mol C mol O₂⁻¹ (Table 3), indicating that
596 suspended POC mineralisation may explain 4.48 ± 0.70% of the inorganic carbon
597 produced following organic matter mineralization in the meso- and bathypelagic waters.



598

599 Figure 7. Full depth distributions of AOU, in $\mu\text{mol kg}^{-1}$ (a), DOC in $\mu\text{mol L}^{-1}$ (b), DON in $\mu\text{mol L}^{-1}$ (c),
 600 POC in $\mu\text{mol L}^{-1}$ (d) and PON in $\mu\text{mol L}^{-1}$ (e) during the FLUXES I cruise. Dots represent samples (AOU
 601 measurements were obtained at 1 db vertical resolution) and vertical black lines represent the corners of
 602 the FLUXES I hydrographic box. Note that depth scale is not linear. The y-axis can be read as station
 603 number (a) or section distance in km (e). Produced with Ocean Data View (Schlitzer, 2017).

604

605 In central waters, no significant differences in POC concentration were found
 606 between transects, except for ENACW with significantly lower POC in the Western
 607 (oceanic) transect ($p < 0.025$) (Table S2, Figure 7d). In intermediate waters, POC had a
 608 subtle increase in the Eastern (coastal) transect, whereas in deep waters a slight increase
 609 was associated to LSW. Per individual transects, the variability of POC explained with
 610 the multiple regression with X_{ij} and AOU was higher than the WT mixing model though
 611 with a small SE reduction of around 5% in the Northern and Southern transects, where
 612 POC represented only $6 \pm 2\%$ and $3 \pm 1\%$ of the inorganic carbon produced by organic
 613 matter mineralization during water mass mixing respectively (Table S3).

615 Table 3. Multiple linear regressions of DOC, DON, POC and PON with the water type proportions (X_{ij})
 616 and AOU or NO_3^- . Determination coefficient (R^2_{+1}), standard deviation (SE_{+1}), percentage of R^2 increase
 617 ($\%R^2$) and percentage of SE reduction ($\%SE$) between the multiple linear regression with X_{ij} (Table 2)
 618 and the multiple linear regression with X_{ij} and AOU or NO_3^- , regression coefficient of each variable with
 619 AOU or NO_3^- (β), and standard error of the estimate (SE_β) and p -value of β .

	DOC vs. AOU	DON vs. AOU	POC vs. AOU	PON vs. AOU	DON vs. NO_3^-	PON vs. NO_3^-
R^2_{+1}	0.70	0.46	0.38	0.44	0.50	0.34
SE_{+1}	3.4	0.7	1.0	0.10	0.73	0.13
$\%R^2$	11	5	46	52	14	17
$\%SE$	15	22	23	23	19	0
β	-0.0260	-0.0130	-0.0325	-0.0034	-0.1568	-0.0210
SE_β	0.0154	0.0035	0.0049	0.0005	0.0246	0.0004
p-level	0.09	0.0003	2.17E-10	4.15E-11	8.4E-10	2.99E-06

620
 621 PON (Figure 7e) generally mirrored the POC distribution in central and
 622 intermediate waters. The multiple regression of PON with X_{ij} explained 29% of its
 623 variance (Table 2) and the inclusion of AOU as explanatory variable increased the
 624 explained variance to 44% with a SE reduction of 23%, while inclusion of NO_3^-
 625 increased the explained variance to 34%. The AOU coefficient was -0.0034 ± 0.001 ,
 626 while NO_3^- coefficient was -0.021 ± 0.004 , meaning that PON covers only $2.1 \pm 0.4\%$
 627 of NO_3^- production following organic matter mineralisation (Table 3).

628
 629 The lowest PON concentrations were found in the Western (oceanic) transect,
 630 while the Northern transect presented two PON maxima in SACW_18 and MMW
 631 (Table S2). In the intermediate and deep WTs, the highest concentrations were observed
 632 in the Eastern (coastal) transect ($p < 0.01$). The variability of PON explained with the

633 multiple regression including X_{ij} and AOU or NO_3^- as explanatory variables was higher
634 in the Southern than in the Northern transect (Table S3), with NO_3^- coefficients of -
635 0.014 ± 0.002 and -0.039 ± 0.010 respectively, indicating that mineralised PON
636 represented $1.4 \pm 0.2\%$ and $3.9 \pm 1.0\%$ of the NO_3^- produced.

637
638 Finally, the C:N molar ratio of POM increased significantly with depth from 9.9
639 ± 1.6 in SACW_18 to 17.3 ± 2.0 in LNEADW (Table 2). In central waters, the
640 maximum C:N molar ratio of POM was observed in SACW_12 and ENACW_12, 12.4 –
641 12.5 , while in the intermediate waters the ratio is similar for the three water masses,
642 ranging from 14.2 to 14.5 . In the deep waters, LNEADW presented the highest C:N
643 molar ratio of POM. Concerning differences between transects, there were not
644 significant differences in the C:N ratio of POM for ENACW_12 (Table S2). In the deep
645 waters, the LSW presented the largest differences in C:N ratio ($p < 0.0005$) being higher
646 in the Western transect (Table S2).

647 648 **4. Discussion**

649 **4.1. Variability in the epipelagic layer of the CVFZ**

650 The relative position of the four transects in relation to the CVF and the proximity
651 of the Mauritanian coast explains the large differences observed in Chl-a levels and
652 depth of the DCM between transects. The depth of the DCM ranged from 33 to 82 m,
653 being deeper and with lower Chl-a concentration in the Western transect, as expected in
654 oligotrophic open ocean waters (Antoine et al., 1996; Mignot et al., 2014; Iuculano et
655 al., 2019). Conversely, the DCM was shallower and with higher Chl-a concentration in
656 the Eastern transect, because of the impact of the offshore export of coastal plankton
657 populations by the Cape Blanc filament (Gabric et al., 1993; Lovecchio et al., 2017;
658 Santana-Falcón et al., 2020). The easternmost part of the Northern transect is
659 dynamically very complex, with both cyclonic and anticyclonic eddies to the West and
660 East of stn 5, respectively (Burgoa et al. in review). The presence of these eddies
661 produces a convergence in stn 5 that generates the movement of the CVF to the North
662 through this station (Figure A10, Burgoa et al. in review). This mesoscale variability at
663 stn 5 of the Northern transect is reflected in the higher concentration of Chl-a. The front
664 interacts with the filament of Cape Blanc, which brought organic matter across the
665 sampling point and generated a hydrographic anomaly around this station, which
666 presents characteristics closer to those observed to the South of the front.

667

668 NH_4^+ and NO_2^- concentrations exhibited several maxima in the surroundings of
669 the DCM. These maxima are associated with the enhanced microbial degradation
670 processes of ammonification and nitrification at the DCM (Ward et al., 1982; Meeder et
671 al., 2012). It has also been suggested that the primary nitrite maximum could be related
672 to inefficient nitrate assimilative reduction by phytoplankton at the low light levels of
673 the DCM (Lomas and Lipschultz, 2006). The mean concentrations of NH_4^+ ($0.06 \mu\text{mol}$
674 kg^{-1}) and NO_2^- ($0.14 \mu\text{mol kg}^{-1}$) found throughout the epipelagic layer of the CVFZ
675 were very low, as expected for oligotrophic waters (Twomey et al., 2007; Li et al.,
676 2008). Higher levels of $0.8 \mu\text{mol kg}^{-1}$ for NH_4^+ and $1.5 \mu\text{mol kg}^{-1}$ for NO_2^- were found
677 in the Eastern (coastal) transect, coinciding again with the offshore export of coastal
678 waters by the filament of Cape Blanc. These levels are comparable with those found by
679 Clark et al. (2016) in the mixed layer of a filament in the Mauritanian upwelling.

680

681 Higher DOC concentrations in the Eastern and Southern transect, i.e. near the
682 coast and South of the CVF, were especially noticeable at the DCM. It is expected that
683 DOC levels are higher when approaching to the coastal ocean (Gattuso et al., 1998; del
684 Giorgio and Duarte, 2002) and can exceed $100 \mu\text{mol L}^{-1}$ in highly productive areas such
685 as in EBUEs (Hill and Wheeler, 2002; Hansell et al., 2009). These high DOC levels can
686 extend offshore due to the horizontal export by the filament of Cape Blanc (Gabric et
687 al., 1993; Lovecchio et al., 2017; 2018). The C:N ratio of DOM was also higher in the
688 Eastern and Southern transects. The mean C:N molar ratio of DOM at the CVFZ (11.7)
689 is slightly higher than the value of $10 \text{ mol C mol N}^{-1}$ found by Church et al. (2002) and
690 Hopkinson and Vallino (2005) in coastal and offshore regions of the North Atlantic and
691 North Pacific central gyre. However, Letscher et al. (2013) found higher values around
692 $16 \text{ mol C mol N}^{-1}$ in the upper 50 m of Eastern Subtropical North Atlantic, (10-40°N 10-
693 50°W) and South Atlantic (10-40°S 10-50°W).

694

695 The highest concentrations of suspended POM were also observed near the coast.
696 Van Camp et al. (1991) and Gabric et al. (1993) estimated that the offshore currents
697 associated with the giant filament could export around 50% of the POM produced in the
698 coastal area around Cape Blanc (21°N). Furthermore, the differences of suspended
699 POM concentration between the Northern and Southern transects could be explained by
700 the passage of CVF across the Northern section around stn 5. The location of the POM

1
2
3
4
5
6
7
8
9
10
11
12
13
14
15
16
17
18
19
20
21
22
23
24
25
26
27
28
29
30
31
32
33
34
35
36
37
38
39
40
41
42
43
44
45
46
47
48
49
50
51
52
53
54
55
56
57
58
59
60
61
62
63
64
65

701 maxima in the Eastern transects coincided with the DCM, while in the Western transect
702 POM maxima were observed at the surface.

703

704 The C:N molar ratio of POM was very variable, being the lowest near the coast
705 i.e. along the Eastern transect (7.6 ± 0.4), because of the intense production of fresh
706 organic matter with a lower C:N ratio in coastal waters and subsequent offshore export
707 by the filament of Cape Blanc. Furthermore, C:N molar ratios to the North of the CVF
708 were higher than to the South and always higher than the canonical Redfield ratio of 6.6
709 (Redfield et al., 1963; Anderson, 1995). In fact, Martiny et al. (2013a, b) showed large
710 spatial variations in the C:N molar ratio of POM in the epipelagic ocean that differed
711 substantially from the classical Redfield ratio, proposing a C:N:P ratio of 137:18:1 in
712 warm, nutrient-rich upwelling zones. This C:N molar ratio of 7.6 is lower than the
713 average value of 8.5, that we found down to the base of the DCM in the CVFZ.

714

715 **4.2. Impact of water mass mixing in meso- and bathypelagic layers**

716 We have applied a water mass analysis to obtain archetype DOC, DON, POC and
717 PON concentrations for the 11 WTs identified during the FLUXES I cruise, for the
718 entire cruise and for each transect. Our water mass analysis followed Pastor et al.
719 (2012), except for the definition of the intermediate water AA and the deep waters.
720 Concerning AA, its physical and chemical properties were taken in the Eastern
721 Equatorial Atlantic, an appropriate source region because this modified Antarctic
722 Intermediate water is transported from the equatorial region to the CVFZ by the
723 Mauritanian current (Figure 1). Conversely, Pastor et al. (2012) took the properties of
724 the AA in the CVFZ. Concerning the deep waters, while Pastor et al. (2012) grouped all
725 deep WTs under the generic denomination of North Atlantic Deep Water (NADW), we
726 identified 3 WTs: UNEADW, LNEADW and LSW, with contrasting origin and silicate
727 concentrations (Pérez-Rodríguez et al., 2001; Álvarez and Álvarez-Salgado, 2009).
728 With regard to the central waters, ENACW and SACW differ in their thermohaline and
729 chemical characteristics as a result of their different origin and history from their
730 respective formation areas to the CVFZ (Stramma and Schott, 1999). ENACW is
731 relatively more ventilated and, therefore, well oxygenated, which explains the
732 contrasting O₂ concentrations in relation to their position with respect to the CVF. The
733 coexistence of the different ENACW and SACW types was evident in the large-scale
734 distribution of water properties in the FLUXES I hydrographic box, as well as at the

735 mesoscale range, with the meandering of the CVF tracing the presence of low salinity
736 central waters of southern origin in some stations of the Northern transect (Figures 3,
737 S1).

738

739 Archetype DOC concentration in ENACW (48 to $52 \mu\text{mol L}^{-1}$) are lower than
740 those found in the Eastern North Atlantic by Álvarez-Salgado et al. (2013) at 40°N and
741 Lønborg and Álvarez Salgado (2014) at 27° – 42°N . This difference could be explained
742 because ENACW at 40°N is closer to the formation area and, therefore younger and
743 DOC-richer, compared to the same water mass at 20°N . However, in intermediate and
744 deep waters, the DOC concentrations were similar to those found by these authors. The
745 archetype DOC concentrations explained a major fraction (63%) of the total DOC
746 variability in the CVFZ, suggesting that mixing and basin-scale mineralisation
747 processes occurring from the formation area to the CVFZ are the main drivers of the
748 DOC variability.

749

750 POC concentrations in the mesopelagic layer of the CVFZ are low, with an
751 average value of $2.0 \pm 0.5 \mu\text{mol L}^{-1}$. Alonso-Gonzalez et al. (2009) reported higher
752 concentrations of suspended POC in the mesopelagic layer of the Canary current from
753 20° to 29°N , (3 – $8 \mu\text{mol L}^{-1}$). This discrepancy is probably due the location of both
754 sampling areas, in the core of the Canary current in Alonso-Gonzalez et al. (2009) and
755 further South in our study. The FLUXES I box is affected by the giant filament of Cape
756 Blanc, where higher contribution of sinking particulate material should be expected
757 (Fischer et al., 2009). Moreover, these high sinking rates are favoured by ballasting
758 effect of atmospheric dust inputs in the area (Bory and Newton, 2000; Fischer and
759 Karakas, 2009). In contrast, POC concentrations in bathypelagic layers of the CVFZ are
760 consistent with what is described by Alonso-Gonzalez et al. (2009).

761

762 The C:N ratios of suspended POM and DOM are higher than the canonical
763 Redfield ratio and increase with depth indicating PON and DON depletion with respect
764 to POC and DOC due to preferential remineralisation of nitrogen-rich compounds
765 (Álvarez-Salgado et al., 2014; Hopkinson and Vallino, 2005; Letscher et al., 2013;
766 Lønborg and Álvarez-Salgado., 2014). Previous research in the study area also found
767 elevated, and sometimes depth dependent, C:N ratios of sinking POM, higher than the
768 Redfield ratio (Fischer et al., 2009; 2016; Nowald et al., 2015), but always lower than

769 the C:N ratios of suspended POM found in this work. The same trend of higher C:N
770 ratios of suspended compared to sinking POM was observed by Schneider et al. (2003)
771 in the subtropical gyre of the North Pacific. We hypothesise that the larger residence
772 time of small size suspended particles in the water column exacerbates the impact of
773 preferential nitrogen mineralisation, explaining the higher C:N molar ratios observed.

774

775 **4.3. Remineralisation of organic matter in the CVFZ**

776 The DOC to AOU ratio obtained from the multiple linear correlation of DOC with
777 the WT proportions and AOU suggests that DOC mineralisation explains only $3.6 \pm$
778 2.1% of the inorganic carbon production in the meso- and bathypelagic waters of the
779 CVFZ. This surprisingly low contribution is well below the 10-20% found by Aristegui
780 et al (2002) for the world ocean, the 26.5% to the south of the Canary Islands obtained
781 by Aristegui et al (2003), the 9-19% obtained by Carlson et al. (2010) in the deep North
782 Atlantic, the $28 \pm 3\%$ found by Alvarez-Salgado et al. (2013) in the subpolar North
783 Atlantic or the $26 \pm 3\%$ by Lønborg and Alvarez-Salgado (2014) in the Eastern North
784 Atlantic from 27° to 42°N . The low contribution of DOC mineralisation in the CVFZ
785 could be explained by 1) the fact that most of the water masses in this region are far
786 away from their formation areas, where the proportion of labile DOC is higher (Hansell
787 et al., 2012; Hansell and Carlson, 2013). In fact, we have shown that archetype DOC
788 concentrations in the ENACW of the CVFZ are significantly lower than in areas closer
789 to the formation area of these WTs (Alvarez-Salgado et al., 2013; Lønborg et al., 2014).
790 And 2) the massive flux of biodegradable sinking POM produced in the coast, which is
791 subjected to lateral export by the giant filament of Cape Blanc and sinks as the filament
792 is moving away from the continental shelf, ballasted lithogenic materials (Iversen et al.,
793 2010; Álvarez-Salgado and Aristegui, 2015; Lovecchio et al., 2018). As recently
794 observed by Lopez et al. (2020) in the Eastern North Pacific, the DOC distribution in
795 the CVFZ is apparently affected by the dissolution of these fast sinking particles, which
796 generate columns of DOC to the bottom.

797

798 In the case of POC, it represents $4.5 \pm 0.7\%$ of the inorganic carbon production of
799 the meso- and bathypelagic waters of the CVFZ. This contribution is far below the
800 estimated by Alonso-González et al. (2009). They estimated that suspended POC
801 transported laterally could account for 28% to 59% of the total mesopelagic respiration
802 in the Canary region. The low contribution in the CVFZ suggests that the respiratory

1
2
3
4
5
6
7
8
9
10
11
12
13
14
15
16
17
18
19
20
21
22
23
24
25
26
27
28
29
30
31
32
33
34
35
36
37
38
39
40
41
42
43
44
45
46
47
48
49
50
51
52
53
54
55
56
57
58
59
60
61
62
63
64
65

803 **organic** carbon demand in the dark ocean is mainly supported by sinking POM. In
804 contrast, suspended POC may be exported rapidly offshore in this area of strong
805 offshore zonal flow, leaving a minor imprint in the biogeochemistry of the study area.
806 This situation contrasts with the Northern location in Alonso-González et al. (2009),
807 where the dominant mean flow is Southward and along-shore with the Canary Current,
808 and the zonal transport is localized in mesoscale filaments and eddies (Lovecchio et al.
809 2017, Álvarez-Salgado et al. 2007).

810
811 The DON to NO_3^- coefficient indicates that **DON supported 16% of NO_3^-**
812 **produced following organic matter mineralisation**. Álvarez-Salgado et al (2006) found
813 that in NW Iberian upwelling (42°N), the contribution of DOM to the mineralisation of
814 organic nitrogen was 30%, while in deep open oceans waters of the North Pacific, **the**
815 **contribution of DON to nitrate production was from 10% to 25%** (Jackson and
816 Williams, 1985; Maita and Yanada, 1990). **Mineralized** PON represented only the $2.1 \pm$
817 0.4% of NO_3^- . As for the case of POC with the oxygen **utilisation**, the maximum
818 contribution of **mineralised** PON to NO_3^- was $3.9 \pm 1.1\%$ in the Northern transect. The
819 higher contributions of **mineralised** DON/PON to NO_3^- than POC/PON to oxygen
820 **utilisation** support the idea that the preferential N remineralisation explains the higher
821 Redfield POM/DOM C:N ratios in the CVFZ.

822

823 **5. Conclusions**

824 The distribution of DOM and suspended POM in the CVFZ is dictated by 1) the
825 position of the front, which separates surface and central waters of contrasting North
826 and South Atlantic origin, and 2) the intersection with meanders of the frontal system
827 associated with mesoscale structures and their interaction with the giant upwelling
828 filament of Cape Blanc. In the intermediate and deep waters, which are very distant
829 from their respective source regions, the distributions are dictated by water mass mixing
830 and remineralization from the source regions to the CVFZ. DOM and suspended POM
831 mineralisation in the study hydrographic box represent only 8.1% of the carbon
832 mineralisation and 17.8% of the nitrogen mineralisation, suggesting that 1) the local
833 carbon demand is mainly supported by sinking POM and 2) N-containing organic
834 compounds are mineralised faster than C-containing organic compounds.

835 The results obtained in this field study confirm a latitudinal gradient in the
836 importance of the vertical vs. horizontal flows of organic matter in the Canary Current

1
2
3
4
5
6
7
8
9
10
11
12
13
14
15
16
17
18
19
20
21
22
23
24
25
26
27
28
29
30
31
32
33
34
35
36
37
38
39
40
41
42
43
44
45
46
47
48
49
50
51
52
53
54
55
56
57
58
59
60
61
62
63
64
65

837 EBUE, and suggest that the offshore regions of EBUEs act as a **transitional** zone that
838 modifies the stoichiometry of the organic matter exported to the gyres, making it poor in
839 nitrogen.

840

841 **Authors' contribution**

842 **S. Valiente:** Methodology, Investigation, Formal analysis, Writing - Original Draft,
843 Visualization. **B. Fernández-Castro:** Methodology, Formal analysis, Investigation,
844 Writing - Review & Editing, Visualization. **R. Campanero:** Investigation, Writing -
845 Review & Editing. **A. Marrero-Díaz:** Data Curation, Investigation, Writing - Review
846 & Editing. **A. Rodríguez-Santana:** Methodology, Investigation, Writing - Review &
847 Editing. **M.D. Gelado-Cabellero:** Methodology, Investigation, Writing - Review &
848 Editing. **M. Nieto-Cid:** Conceptualization, Methodology, Investigation, Writing -
849 Review & Editing. **A. Delgado-Huertas:** Conceptualization, Writing - Review &
850 Editing, Supervision, Funding acquisition. **J. Arístegui:** Conceptualization,
851 Methodology, Investigation, Writing - Review & Editing, Project administration,
852 Funding acquisition. **X.A. Álvarez-Salgado:** Conceptualization, Methodology, Formal
853 analysis, Investigation, Writing - Original Draft, Writing - Review & Editing,
854 Visualization, Supervision, Project administration, Funding acquisition

855

856 **Acknowledgements**

857 We would like to thank the captain and crew of R/V Sarmiento de Gamboa and
858 the personnel of the CSIC Unidad de Tecnología Marina (UTM), for their help during
859 the FLUXES I cruise, as well as to M.J. Pazo for DOM and POM analysis and V.
860 Vieitez for nutrient and POM analyses. This work was supported by Spanish National
861 Science Plan research grants FLUXES (CTM2015-69392-C3) and e-IMPACT
862 (PID2019-109084RB-C2). S.V.R and R.C.N were supported by PhD fellowships from
863 the Spanish Ministry of Science and Innovation (BES-2016-079216 and BES-2016-
864 076462); B.F.C was supported by a Juan de La Cierva Formación fellowship (FJCI-
865 641-2015-25712) and by the European Union's Horizon 2020 research and
866 innovation program under the Marie Skłodowska-Curie grant agreement No.
867 834330 (SO-CUP). M.N.-C. was partially supported by the project FERMIO
868 (MINECO, CTM2014-57334-JIN), co-financed with FEDER funds. J.A. was
869 partly supported by the project SUMMER (AMD-817806-5) from the European
870 Union's Horizon 2020 research and innovation program.

871 **References**

- 872 Alonso-González, I.J., Arístegui, J., Vilas, J.C., Hernández-Guerra, A., 2009. Lateral
873 POC transport and consumption in surface and deep waters of the Canary Current
874 region: A box model study. *Global Biogeochem. Cycles* 23, GB2007.
875 <https://doi.org/10.1029/2008GB003185>
- 876 Alpers, W., Brandt, P., Lazar, A., Dagorne, D., Sow, B., Faye, S., Hansen, M.W.,
877 Rubino, A., Poulain, P.M., Brehmer, P., 2013. A small-scale oceanic eddy off the
878 coast of West Africa studied by multi-sensor satellite and surface drifter data.
879 *Remote Sens. Environ.* 129, 132–143. <https://doi.org/10.1016/j.rse.2012.10.032>
- 880 Álvarez-Salgado, X.A., Arístegui, J., Barton, E.D., Hansell, D.A., 2007. Contribution of
881 upwelling filaments to offshore carbon export in the subtropical Northeast Atlantic
882 Ocean. *Limnol. Oceanogr.* 52, 1287–1292.
883 <https://doi.org/10.4319/lo.2007.52.3.1287>
- 884 Álvarez-Salgado, X.A., Nieto-Cid, M., Gago, J., Brea, S., Castro, C.G., Doval, M.D.,
885 Pérez, F.F., 2006. Stoichiometry of the degradation of dissolved and particulate
886 biogenic organic matter in the NW Iberian upwelling. *J. Geophys. Res.* 111,
887 C07017. <https://doi.org/10.1029/2004JC002473>
- 888 Álvarez-Salgado, X., Arístegui, J., 2015. Organic matter dynamics in the Canary
889 Current. L. Vald. I. Déniz-González (Eds.), *Oceanogr. Biol. Featur. Canar. Curr.*
890 *Large Mar. Ecosyst. IOC-UNESCO, Paris (2015)*, pp. 151-160 (IOC Tech. Ser.
891 No. 115).
- 892 Álvarez-Salgado, X., Nieto-Cid, M., Álvarez, M., Pérez, F., Morin, P., Mercier, H.,
893 2013. New insights on the mineralization of dissolved organic matter in central,
894 intermediate, and deep water masses of the northeast North Atlantic. *Limnol.*
895 *Oceanogr.* 58, 681–696. <https://doi.org/10.4319/lo.2013.58.2.0681>
- 896 Álvarez, M., Álvarez-Salgado, X., 2009. Chemical tracer transport in the eastern
897 boundary current system of the North Atlantic. *Ciencias Mar.* 35, 123–139.
898 <https://doi.org/10.7773/cm.v35i2.1438>
- 899 Álvarez, M., Brea, S., Mercier, H., Álvarez-Salgado, X., 2014. Mineralization of
900 biogenic materials in the water masses of the South Atlantic Ocean. I: Assessment
901 and results of an optimum multiparameter analysis. *Prog. Oceanogr.* 123, 1–23.
902 <https://doi.org/10.1016/j.pocean.2013.12.007>
- 903 Anderson, L.A., 1995. On the hydrogen and oxygen content of marine phytoplankton.
904 *Deep. Res. Part I* 42, 1675–1680. [https://doi.org/10.1016/0967-0637\(95\)00072-E](https://doi.org/10.1016/0967-0637(95)00072-E)

- 1
2
3
4
5
6
7
8
9
10
11
12
13
14
15
16
17
18
19
20
21
22
23
24
25
26
27
28
29
30
31
32
33
34
35
36
37
38
39
40
41
42
43
44
45
46
47
48
49
50
51
52
53
54
55
56
57
58
59
60
61
62
63
64
65
- 905 Antoine, D., Andre, J.M., Morel, A., 1996. Oceanic primary production: 2. Estimation
906 at global scale from satellite (Coastal Zone Color Scanner) chlorophyll. *Global*
907 *Biogeochem. Cycles* 10, 57–69. <https://doi.org/10.1029/95GB02832>
- 908 Arístegui, J., Barton, E., Montero, M., García-Muñoz, M., Escáñez, J., 2003. Organic
909 carbon distribution and water column respiration in the NW Africa-Canaries
910 Coastal Transition Zone. *Aquat. Microb. Ecol.* 33, 289–301.
- 911 Arístegui, J., Barton, E.D., Álvarez-Salgado, X.A., Santos, A., Figueiras, F.G., Kifani,
912 S., Hernández-León, S., Mason, E., Machú, E., Demarcq, H., 2009. Sub-regional
913 ecosystem variability in the Canary Current upwelling. *Prog. Oceanogr.* 83, 33–48.
914 <https://doi.org/10.1016/j.pocean.2009.07.031>
- 915 Arístegui, J., Duarte, C., Agustí, S., Doval, M., Álvarez-Salgado, X., Hansell, D.A.,
916 2002. Dissolved Organic Carbon Support of Respiration in the Dark Ocean. *Sci.*
917 298, 967.
- 918 Arístegui, J., Montero, M., Hernández-Hernández, N., Alonso-González, I., Baltar, F.,
919 Calleja, M.L., Duarte, C.M., 2020. Variability in Water-Column Respiration and
920 Its Dependence on Organic Carbon Sources in the Canary Current Upwelling
921 Region. *Front. Earth Sci.* 8, 349. <https://doi.org/10.3389/feart.2020.00349>
- 922 Barceló-Llull, B., Sangrà, P., Pallàs-Sanz, E., Barton, E.D., Estrada-alls, S.N.,
923 Martínez-Marrero, A., Aguiar-Gonzalez, B., Grisolla, D., Gordo, C., Rodríguez-
924 Santana, Á., Marrero-Díaz, Á., Arístegui, J., 2017. Anatomy of a subtropical
925 intrathermocline eddy. *Deep. Res. Part I Oceanogr. Res. Pap.* 124, 126–139.
- 926 Barton, E., Arístegui, J., Tett, P., Cantón, M., García- Braun, J., Hernández-León, S.,
927 Nykjaer, L., Almeida, C., Almunia, J., Ballesteros, S., Basterretxea, G., Escáñez,
928 J., García-Weil, L., Hernandez-Guerra, A., López-Laatzén, F., Molina, R.,
929 Montero, M., Navarro-Pérez, E., Rodríguez, J., Van Lenning, K., Wild, K., 1998.
930 The transition zone of the Canary Current upwelling region. *Prog. Oceanogr.* 41,
931 455–504.
- 932 Bory, A.J.-M., Newton, P.P., 2000. Transport of airborne lithogenic material down
933 through the water column in two contrasting regions of the eastern subtropical
934 North Atlantic Ocean. *Global Biogeochem. Cycles* 14, 297–315.
935 <https://doi.org/10.1029/1999gb900098>
- 936 Boyd, P., Claustre, H., Levy, M., Siegel, D., Weber, T., 2019. Multi-faceted particle
937 pumps drive carbon sequestration in the ocean. *Nature* 568, 327–336.
- 938 Broecker, W.S., 1974. NO a conservative water–mass tracer. *Earth Planet. Sci. Lett.* 23

939 100–107.

940 Burgoa, N., Machín, F., Marrero-Díaz, S., Rodríguez-Santana, A., Martínez-Marrero,
941 A., Arístegui, J., Duarte, C., 2020. Mass, nutrients and dissolved organic carbon
942 (DOC) lateral transports off northwest Africa during fall 2002 and spring 2003
943 Item Type Article. *Ocean Sci.* 16, 483–511. [https://doi.org/10.5194/os-16-483-](https://doi.org/10.5194/os-16-483-2020)
944 2020

945 Cardoso, C., Caldeira, R.M.A., Relvas, P., Stegner, A., 2020. Islands as eddy
946 transformation and generation hotspots: Cabo Verde case study. *Prog. Oceanogr.*
947 184, 102271. <https://doi.org/10.1016/j.pocean.2020.102271>

948 Carlson, C., Hansell, D., Nelson, N., Siegel, D., 2010. Dissolved organic carbon export
949 and subsequent remineralization in the mesopelagic and bathypelagic realms of the
950 North Atlantic basin. *Deep Sea Res. Part II* 57, 1433–1445.

951 Church, M.J., Ducklow, H.W., Karl, D.M., 2002. Multiyear increases in dissolved
952 organic matter inventories at Station ALOHA in the North Pacific Subtropical
953 Gyre. *Limnol. Oceanogr.* 47, 1–10. <https://doi.org/10.4319/lo.2002.47.1.0001>

954 Clark, D.R., Widdicombe, C.E., Rees, A.P., Woodward, E., 2016. The significance of
955 nitrogen regeneration for new production within a filament of the Mauritanian
956 upwelling system. *Biogeosciences* 13, 2873–2888. [https://doi.org/10.5194/bg-13-](https://doi.org/10.5194/bg-13-2873-2016)
957 2873-2016

958 Del Giorgio, P., Duarte, C., 2002. Respiration in the open ocean. *Nature* 420, 379–384.

959 Fischer, G., Karakaş, G., 2009. Sinking rates and ballast composition of particles in the
960 Atlantic Ocean: implications for the organic carbon fluxes to the deep ocean.
961 *Biogeosciences* 6, 85–102. <https://doi.org/10.5194/bg-6-85-2009>

962 Fischer, G., Reuter, C., Karakas, G., Nowald, N., Wefer, G., 2009. Offshore advection
963 of particles within the Cape Blanc filament, Mauritania: Results from observational
964 and modelling studies. *Prog. Oceanogr.* 83, 322–330.

965 Fischer, G., Romero, O., Toby, E., Iversen, M., Donner, B., Mollenhauer, G., Nowald,
966 N., Ruhland, G., Klann, M., Hamady, B., Wefer, G., 2019. Changes in the Dust-
967 Influenced Biological Carbon Pump in the Canary Current System: Implications
968 From a Coastal and an Offshore Sediment Trap Record Off Cape Blanc,
969 Mauritania. *Global Biogeochem. Cycles* 33, 1100–1128.
970 <https://doi.org/10.1029/2019GB006194>

971 Gabric, A.J., Garcia, L., Van Camp, L., Nykjaer, L., Eifler, W., Schrimpf, W., 1993.
972 Offshore export of shelf production in the Cape Blanc (Mauritania) giant filament

1 973 as derived from coastal zone color scanner imagery. *J. Geophys. Res.* 98, 4697–
2 974 4712. <https://doi.org/10.1029/92JC01714>

3 975 Gattuso, J.-P., Frankignoulle, M., Wollast, R., 1998. Carbon and Carbonate metabolism
4 976 in coastal aquatic ecosystems. *Annu. Rev. Ecol. Syst.* 29, 405–434.
5 977 <https://doi.org/10.1146/annurev.ecolsys.29.1.405>

6 978 Hansell, D.A., Carlson, C.A., 2013. Localized refractory dissolved organic carbon sinks
7 979 in the deep ocean. *Global Biogeochem. Cycles* 27, 705–710.
8 980 <https://doi.org/10.1002/gbc.20067>

9 981 Hansell, D.A., Carlson, C.A., Schlitzer, R., 2012. Net removal of major marine
10 982 dissolved organic carbon fractions in the subsurface ocean. *Global Biogeochem.*
11 983 *Cycles* 26, GB1016. <https://doi.org/10.1029/2011GB004069>

12 984 Hansell, D., Carlson, C., Repeta, D., Schlitzer, R., 2009. Dissolved organic matter in the
13 985 ocean: A controversy stimulates new insights. *Oceanography* 22, 202–211.

14 986 Hansen, H., Koroleff, F., 1999. *Methods of Seawater Analysis*, 3rd, Completely
15 987 Revised and Extended Edition, Ed. by K. Grashoff et al (Wiley, Weinheim, 1999),
16 988 pp. 149–228.

17 989 Helmke, P., Romero, O., Fischer, G., 2005. Northwest African upwelling and its effect
18 990 on offshore organic carbon export to the deep sea. *Global Biogeochem. Cycles* 19,
19 991 GB4015. <https://doi.org/10.1029/2004GB002265>

20 992 Hill, J.K., Wheeler, P.A., 2002. Organic carbon and nitrogen in the northern California
21 993 current system: comparison of offshore, river plume, and coastally upwelled
22 994 waters. *Prog. Oceanogr.* 53, 369–387.

23 995 Holm-Hansen, O., Lorenzen, C.J., Holmes, R.W., Strickland, J.D.H., 1965.
24 996 Fluorometric Determination of Chlorophyll. *ICES J. Mar. Sci.* 30, 3–15.
25 997 <https://doi.org/10.1093/icesjms/30.1.3>

26 998 Hopkinson, C., Vallino, J., 2005. Efficient export of carbon to the deep ocean through
27 999 dissolved organic matter. *Nature* 433, 142–145.

28 1000 Iuculano, F., Álvarez-Salgado, X., Otero, J., Catalá, T., Sobrino, C., Duarte, C., Agustí,
29 1001 S., 2019. Patterns and drivers of UV absorbing chromophoric dissolved organic
30 1002 matter in the euphotic layer of the open ocean. *Front. Mar. Sci.* 6, 320.

31 1003 Iversen, M., Nowald, N., Ploug, H., Jackson, G., Fischer, G., 2010. High resolution
32 1004 profiles of vertical particulate organic matter export off Cape Blanc, Mauritania:
33 1005 Degradation processes and ballasting effects. *Deep. Res. Part I* 57, 771–784.

34 1006 Jackson, G.A., Williams, P.M., 1985. Importance of dissolved organic nitrogen and

- 1007 phosphorus to biological nutrient cycling. *Deep Sea Res. Part A, Oceanogr. Res.*
1008 Pap. 32, 223–235. [https://doi.org/10.1016/0198-0149\(85\)90030-5](https://doi.org/10.1016/0198-0149(85)90030-5)
- 1009 Karakaş, G., Nowald, N., Blaas, M., Marchesiello, P., Frickenhaus, S., Schlitzer, R.,
1010 2006. High-resolution modeling of sediment erosion and particle transport across
1011 the northwest African shelf. *J. Geophys. Res.* 111, C06025.
1012 <https://doi.org/10.1029/2005JC003296>
- 1013 Karstensen, J., Tomczak, M., 1998. Age determination of mixed water masses using
1014 CFC and oxygen data. *J. Geophys. Res.* 103, 18599–18609.
1015 <https://doi.org/10.1029/98JC00889>
- 1016 K  rouel, R., Aminot, A., 1997. Fluorometric determination of ammonia in sea and
1017 estuarine waters by direct segmented flow analysis. *Mar. Chem.* 57, 265–275.
1018 [https://doi.org/10.1016/S0304-4203\(97\)00040-6](https://doi.org/10.1016/S0304-4203(97)00040-6)
- 1019 Langdon, C., 2010. Determination of dissolved oxygen in seawater by winkler titration
1020 using the amperometric technique. Hood, E.M., Sloyan, B.M., Sabine, C. (Eds.),
1021 Go-sh. Repeat Hydrogr. Man. A Collect. Expert Reports Guidel. IOCCP Rep. no.
1022 14, ICPO Publ. Ser. no. 134.
- 1023 Letscher, R.T., Hansell, D.A., Carlson, C.A., Lumpkin, R., Knapp, A.N., 2013.
1024 Dissolved organic nitrogen in the global surface ocean: Distribution and fate.
1025 *Global Biogeochem. Cycles* 27, 141–153. <https://doi.org/10.1029/2012GB004449>
- 1026 Li, Q.P., Hansell, D.A., Zhang, J.-Z., 2008. Underway monitoring of nanomolar nitrate
1027 plus nitrite and phosphate in oligotrophic seawater. *Limnol. Oceanogr. Methods* 6,
1028 319–326. <https://doi.org/10.4319/lom.2008.6.319>
- 1029 Lomas, M.W., Lipschultz, F., 2006. Forming the primary nitrite maximum: Nitrifiers or
1030 phytoplankton? *Limnol. Oceanogr.* <https://doi.org/10.4319/lo.2006.51.5.2453>
- 1031 L  nborg, C. and,   lvarez-Salgado, 2014. Tracing dissolved organic matter cycling in
1032 the eastern boundary of the temperate North Atlantic using absorption and
1033 fluorescence spectroscopy. *Deep. Res. I* 85, 35–46.
- 1034 Lopez, C.N., Robert, M., Galbraith, M., Bercovici, S.K., Orellana, M. V., Hansell, D.A.,
1035 2020. High Temporal Variability of Total Organic Carbon in the Deep
1036 Northeastern Pacific. *Front. Earth Sci.* 8, 80.
1037 <https://doi.org/10.3389/feart.2020.00080>
- 1038 Lovecchio, E., Gruber, N., M  nnich, M., 2018. Mesoscale contribution to the long-
1039 range offshore transport of organic carbon from the Canary Upwelling System to
1040 the open North Atlantic. *Biogeosciences* 15, 2018–5061.

- 1041 <https://doi.org/10.3929/ethz-b-000286944>
- 1042 Lovecchio, E., Gruber, N., Münnich, M., Lachkar, Z., 2017. On the long-range offshore
1043 transport of organic carbon from the Canary Upwelling System to the open North
1044 Atlantic. *Biogeosciences* 14, 3337–3369. [https://doi.org/10.3929/ethz-b-](https://doi.org/10.3929/ethz-b-000190480)
1045 [000190480](https://doi.org/10.3929/ethz-b-000190480)
- 1046 Maita, Y., Yanada, M., 1990. Vertical distribution of total dissolved nitrogen and
1047 dissolved organic nitrogen in seawater. *Geochem. J.* 24, 245–254.
1048 <https://doi.org/10.2343/geochemj.24.245>
- 1049 Martínez-Marrero, A., Rodríguez-Santana, A., Hernández-Guerra, A., Fraile-Nuez, E.,
1050 López-Laatzén, F., Vélez-Belchí, P., Parrilla, G., 2008. Distribution of water
1051 masses and diapycnal mixing in the Cape Verde Frontal Zone. *Geophys. Res. Lett.*
1052 35, L07609. <https://doi.org/10.1029/2008GL033229>
- 1053 Martiny, A., Vrugt, J., Primeau, F., Lomas, M., 2013. Regional variation in the
1054 particulate organic carbon to nitrogen ratio in the surface ocean. *Global*
1055 *Biogeochem. Cycles* 27, 723–731. <https://doi.org/10.1002/gbc.20061>
- 1056 Martiny, A.C., Pham, C.T.A., Primeau, F.W., Vrugt, J.A., Moore, J.K., Levin, S.A.,
1057 Lomas, M.W., 2013. Strong latitudinal patterns in the elemental ratios of marine
1058 plankton and organic matter. *Nat. Geosci.* 6, 279–283.
1059 <https://doi.org/10.1038/ngeo1757>
- 1060 Meeder, E., Mackey, K., Paytan, A., Shaked, Y., Iluz, D., Stambler, N., Rivlin, T., Post,
1061 A., Lazar, B., 2012. Nitrite dynamics in the open ocean—clues from seasonal and
1062 diurnal variations. *Mar. Ecol. Prog. Ser.* 453, 11–26.
1063 <https://doi.org/10.3354/meps09525>
- 1064 Meunier, T., Barton, E., Barreiro, B., Torres, R., 2012. Upwelling filaments off cap
1065 blanc: Interaction of the NW african upwelling current and the cape verde frontal
1066 zone eddy field? *J. Geophys. Res.* 117, C08031.
1067 <https://doi.org/10.1029/2012JC007905>
- 1068 Mignot, A., Claustre, H., Uitz, J., Poteau, A., D’Ortenzio, F., Xing, X., 2014.
1069 Understanding the seasonal dynamics of phytoplankton biomass and the deep
1070 chlorophyll maximum in oligotrophic environments: A Bio-Argo float
1071 investigation. *Global Biogeochem. Cycles* 28, 856– 876.
1072 <https://doi.org/10.1002/2013GB004781>
- 1073 Nowald, N., Iversen, M., Fischer, G., Ratmeyer, V., Wefer, G., 2015. Time series of in-
1074 situ particle properties and sediment trap fluxes in the coastal upwelling filament

- 1075 off Cape Blanc, Mauritania. *Prog. Oceanogr.* 137, 1–11.
- 1076 <https://doi.org/10.1016/j.pocean.2014.12.015>
- 1077 Nowald, N., Karakas, G., Ratmeyer, V., Fischer, G., Schlitzer, R., Davenport, R.A.,
1078 Wefer, G., 2006. Distribution and transport processes of marine particulate matter
1079 off Cape Blanc (NW-Africa): results from vertical camera profiles. *Ocean Sci.*
1080 *Discuss* 3, 903–938.
- 1081 Ohde, T., Fiedler, B., Körtzinger, A., 2015. Spatio-temporal distribution and transport
1082 of particulate matter in the eastern tropical North Atlantic observed by Argo floats.
1083 *Deep. Res. Part I* 102, 26–42.
- 1084 Olivar, M., Sabatés, A., Pastor, M., Pelegrí, J., 2016. Water masses and mesoscale
1085 control on latitudinal and cross-shelf variations in larval fish assemblages off NW
1086 Africa. *Deep. Res. Part I Oceanogr. Res. Pap.* 117, 120–137.
1087 <https://doi.org/10.1016/j.dsr.2016.10.003>
- 1088 Pastor, M., Peña-Izquierdo, J., Pelegrí, J., Marrero-Díaz, A., 2012. Meridional changes
1089 in water mass distributions off NW Africa during November 2007/2008. *Ciencias*
1090 *Mar.* 38, 223– 244. <https://doi.org/10.7773/cm.v38i1B.1831>
- 1091 Pelegrí, J.L., Peña-Izquierdo, J., 2015. Easter boundary currents off North' West Africa.
1092 *Oceanogr. Biol. Featur. Canar. Curr. Large Mar. Ecosyst.* 3 81-92 , IOC Tech. Ser.
1093 115 81–92 IOC Technical Series.
- 1094 Pérez-Rodríguez, P., Pelegrí, J., Marrero-Díaz, A., 2001. Dynamical characteristics of
1095 the Cape Verde frontal zone. *Mar. Sci.* 65, 241–250.
- 1096 Redfield, A.C., Ketchum, B., Richards, F., 1963. The influence of organisms on the
1097 composition of seawater. “The Sea” (Hill, M. N., ed.). Vol. 2, Wiley-
1098 Interscience, New York. pp. 26–77. Richards, F. A.
- 1099 Repeta, D.J., 2015. Chemical Characterization and Cycling of Dissolved Organic
1100 Matter, in: *Biogeochemistry of Marine Dissolved Organic Matter: Second Edition.*
1101 Elsevier Inc., pp. 21–63. <https://doi.org/10.1016/B978-0-12-405940-5.00002-9>
- 1102 Sangrà, P., Pascual, A., Rodríguez-Santana, Á., Machín, F., Mason, E., McWilliams,
1103 J.C., Pelegrí, J.L., Dong, C., Rubio, A., Arístegui, J., Marrero-Díaz, Á.,
1104 Hernández-Guerra, A., Martínez-Marrero, A., Auladell, M., 2009. The Canary
1105 Eddy Corridor: A major pathway for long-lived eddies in the subtropical North
1106 Atlantic. *Deep. Res. Part I Oceanogr. Res. Pap.* 56, 2100–2114.
1107 <https://doi.org/10.1016/j.dsr.2009.08.008>
- 1108 Santana-Falcón, Y., Mason, E., Arístegui, J., 2020. Offshore transport of organic carbon

- 1109 by upwelling filaments in the Canary Current System. *Prog. Oceanogr.* 186,
1110 102322. <https://doi.org/10.1016/j.pocean.2020.102322>
- 1111 Schlitzer, R., 2017. Ocean Data View. Ocean Data View.
- 1112 Schneider, B., Schlitzer, R., Fischer, G., Nöthig, E.M., 2003. Depth-dependent
1113 elemental compositions of particulate organic matter (POM) in the ocean. *Global*
1114 *Biogeochem. Cycles* 17. <https://doi.org/10.1029/2002gb001871>
- 1115 Stramma, L., Schott, F., 1999. The mean flow field of the tropical Atlantic Ocean.
1116 *Deep. Res. II* 46, 279–303.
- 1117 Tiedemann, M., Fock, H., Döring, J., Bonaventure-Badji, L., Möllmann, C., 2018.
1118 Water masses and oceanic eddy regulation of larval fish assemblages along the
1119 Cape Verde Frontal Zone. *J. Mar. Syst.* 183, 42–55.
- 1120 Tomczak, M., 1999. Some historical, theoretical and applied aspects of quantitative
1121 water mass analysis. *J. Mar. Res.* 57, 275–303.
1122 <https://doi.org/10.1357/002224099321618227>
- 1123 Twomey, L.J., Waite, A.M., Pez, V., Pattiaratchi, C.B., 2007. Variability in nitrogen
1124 uptake and fixation in the oligotrophic waters off the south west coast of Australia.
1125 *Deep. Res. Part II Top. Stud. Oceanogr.* 54, 925–942.
1126 <https://doi.org/10.1016/j.dsr2.2006.10.001>
- 1127 UNESCO, 1986. Progression Oceanographic Tables and Standards 1983–1986. Work
1128 and Recommendations of the UNESCO/SCOR/ICES/IAPSO Joint Panel. UNESCO
1129 Technical Papers in Marine Science 50.
- 1130 Van Camp, L., Nykjaer, L., Mittelstaedt, E., Schlittenhardy, P., 1991. Upwelling and
1131 boundary circulation off Northwest Africa as depicted by infrared and visible
1132 satellite observations. *Prog. Oceanogr.* 26, 357–402.
- 1133 Verdugo, P., Alldredge, A.L., Azam, F., Kirchman, D.L., Passow, U., Santschi, P.H.,
1134 2004. The oceanic gel phase: a bridge in the DOM-POM continuum. *Mar. Chem.*
1135 92, 67–85. <https://doi.org/10.1016/j.marchem.2004.06.017>
- 1136 Ward, B.B., Olson, R.J., Perry, M.J., 1982. Microbial nitrification rates in the primary
1137 nitrite maximum off southern California. *Deep Sea Res. Part A, Oceanogr. Res.*
1138 *Pap.* 29, 247–255. [https://doi.org/10.1016/0198-0149\(82\)90112-1](https://doi.org/10.1016/0198-0149(82)90112-1)
- 1139 Zenk, W., Klein, B., Schroder, M., 1991. Cape Verde Frontal Zone. *Deep Sea Res. Part*
1140 *A* 38, S505–S530. [https://doi.org/10.1016/S0198-0149\(12\)80022-7](https://doi.org/10.1016/S0198-0149(12)80022-7)
- 1141

Declaration of interests

The authors declare that they have no known competing financial interests or personal relationships that could have appeared to influence the work reported in this paper.

The authors declare the following financial interests/personal relationships which may be considered as potential competing interests:

1
2
3
4
5
6
7
8
9
10
11
12
13
14
15
16
17
18
19
20
21
22
23
24
25
26
27
28
29
30
31
32
33
34
35
36
37
38
39
40
41
42
43
44
45
46
47
48
49
50
51
52
53
54
55
56
57
58
59
60
61
62
63
64
65

[Click here to access/download](#)

e-Component

Supplementary Material, Valiente et al.docx